ChemComm

Accepted Manuscript

This article can be cited before page numbers have been issued, to do this please use: D. Rota Martir and E. Zysman-Colman, *Chem. Commun.*, 2018, DOI: 10.1039/C8CC08327D.

ROYAL SOCIETY OF CHEMISTRY

rsc.li/chemcomm

Photoactive Supramolecular Cages Incorporating Ru(II) and Ir(III) Metal Complexes

Diego Rota Martir[a] *and Eli Zysman-Colman*[a]*

[a] Organic Semiconductor Centre, EaStCHEM School of Chemistry, University of St Andrews, St Andrews, Fife, KY16 9ST, UK, Fax: +44-1334 463808; Tel: +44-1334 463826; E-mail: eli.zysman-colman@st-andrews.ac.uk; URL: http://www.zysman-colman.com

Abstract. The self-assembly of arrays of metal ions with bridging ligands has evolved during the last twenty years as a powerful approach for the construction of cages and capsules with well-defined shapes and cavities. There has been of late an increasing exploration of photoactive supramolecular cages in which at least one component, either the metal ion or the ligands, themselves incorporating metal complexes (metalloligands), are phosphorescent. Desirable photophysical properties such as emission tuning and encapsulation-assisted energy and electron transfer have been achieved by integrating phosphorescent *d*-block Ir(III) and Ru(II) complexes into the backbone of metallosupramolecular cages and capsules. Such cages have been used in sensing applications, photocatalysis and in the context of solar fuels production. This feature article summarises the recent work on cage assemblies containing Ir(III) and Ru(II) metal complexes as photoactive units, highlighting our contribution to this growing field and bringing together our key results.

Introduction

Coordination cages and capsules, formed through the self-assembly of arrays of metal ions and bridging ligands, have been one of the main areas of interest in supramolecular chemistry over the last two decades.[1] Coordination-driven self-assembly, which is based on metal-ligand

coordination chemistry, has rapidly matured as a powerful approach for the construction of discrete two-dimensional (2-D) metallocycles and three-dimensional (3-D) metallocages and capsules with well-defined shapes, geometries and cavities.[2] In this context, the groups of Lehn,[3] Stang,[4] Fujita,[5] Raymond,[6] Newkome,[7] Nitschke[8] and others[9] have successfully pioneered a number of methodologies to construct numerous topologically trivial metallosupramolecular architectures. They have shown that the relatively strong and highly directional metal-ligands bonds can program the coordination-driven self-assembly process towards defined shapes and topologies of the resultant structures, frequently in high yields and short reaction times. The self-assembly between palladium(II) or platinum(II) metal ions and ligands containing specifically positioned distal pyridine moieties, first demonstrated by Fujita and co-workers,[10] is one of the most popular and successful strategies to prepare molecular cages and capsules.[1c, 8, 11] The first example of a coordination-driven molecular cage was a small $[M_6L_4]^{12+}$ tetrahedron, where M is either a Pd(II) or Pt(II) metal ion located at each vertex of the tetrahedron and L is a bridging ligand, specifically the electron-poor 2,4,6-tris(pyridin-4-yl-1,3,5-triazine), spanning each of the six edges.[10, 12] More recently, by assembling bis-pyridyl bridging ligands characterized by extended curvatures with Pd^{2+} ions, large $[Pd_{12}L_{24}]^{24+}$,[13] $[Pd_{24}L_{48}]^{48+}$,[5] and huge $[Pd_{30}L_{60}]^{60+}$ "nanospheres"[14] have been rationally designed (Figure **1**). Such cages represent a fascinating synthetic challenge as they illustrate how, with careful control of the bridging ligand geometry and the type of metal ion, remarkably elaborate and highly symmetric structures can be successfully formed using self-assembly.[1a, 1c, 8, 11f]

View Article Online
DOI: 10.1039/C8CC08327D

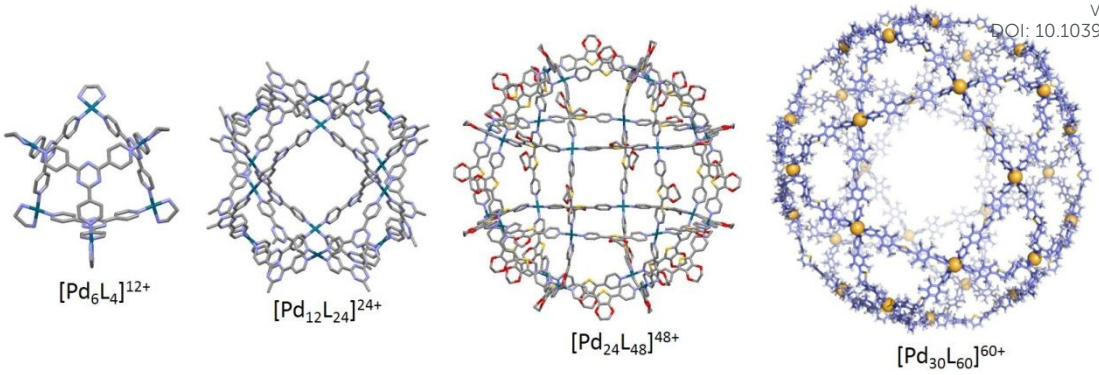

Figure **1**. X-ray structures of cage $[Pd_4L_6]^{12+}$ and nanospheres $[Pd_{12}L_{24}]^{24+}$, $[Pd_{24}L_{48}]^{48+}$ and $[Pd_{30}L_{60}]^{60+}$, respectively from left to right.

As the field of coordination cage assembly has matured, the focus has more recently shifted increasingly towards the design of cages with defined function and the investigation of their properties.[1d, 11f, 15] Small guest molecules have been shown to be selectively sequestrated inside the cavities of these cages and their host-guest interactions have been exploited in diverse applications such as "artificial enzyme" catalysis,[16] for hazardous chemical capture and reactive intermediate stabilization,[17] for drug delivery and release,[18] as well as in molecular sensing[19] and biology.[20] The functional properties of these cages are frequently derived from the incorporation of functional groups into the organic building blocks.[21] For example, Stang and co-workers have successfully introduced various functional moieties, such as ferrocene,[22] crown-ethers[23] and dendrons[24] at the vertex of building blocks, which enabled the construction of a series of functional metallomacrocycles. Lutzen and co-workers introduced 2,2'-dihydroxy-1,1'-binaphtyl (BINOL) as chiral units into molecular cages of composition $[Pd_4L_8]^{8+}$, $[Pd_6L_{12}]^{12+}$ and $[Pd_{12}L_{24}]^{24+}$.[25] Yoshizawa and co-workers introduced electro- and magneto-chemical dihydrophenazine derivatives that can form stable radical cations by single-electron oxidation under ambient conditions into cage compounds of the composition of $[Pd_2L_4]^{4+}$.[26] Clever and co-workers[27] have reported a series of $[Pd_2L_4]^{4+}$ coordination cages, but featuring endohedral functionalities consisting of two electron-withdrawing substituents

(CO_2R and/or CN) attached to an electron-rich backbone via a double bond that behave as push-pull molecular rotors. Lutzen, Clever and co-workers[28] have also recently reported a $[Pd_6L_{12}]^{12+}$ cage containing a luminescent BODIPY-based bis(3-pyridyl) ligand that possesses a rotaxane-like cage-in-ring arrangement.

A recent area of considerable interest is the design and development of photoactive cages and capsules in which either the metal ion or the bridging ligand is luminescent.[21a, 29] Such cages provide both a high concentration of chromophores and defined cavities to govern the host-guest optoelectronic interactions. This immediately opens the door to many possible applications such as sensing and photocatalysis involving bound guests that can photophysically interact with the emitting hosts. Indeed, incorporation of fluorescent emitters such as porphyrins and BODIPYs,[19a, 30] π-conjugated organic compounds,[31] and more recently thermally activated delayed fluorescent emitters (TADF)[32] into the ligand backbone of cages and macrocycles have been shown to give rise to luminescent cages and macrocycles.[29b, 30c, 33] Less studied are supramolecular cages incorporating *d*-block transition metal complexes such as ruthenium(II), iridium(III), platinum(II), rhenium(I), gold(I), silver(I), rhodium(III) and osmium(II) complexes. Of these metals, the majority of recent interest has focused on the investigation of photoactive supramolecular cages incorporating luminescent Ir(III) and Ru(II) metal complexes. The resulting cages have been shown to possess a highly desirable set of optoelectronic and physical properties including wide color tunability, relatively high photoluminescence quantum yields (Φ_{PL}) with short phosphorescence lifetime (τ_{PL}) and high chemical stability. They have been primarily used as sensors and as supramolecular photocatalysts for cavity-directed chemical transformations of bound guests and for hydrogen production. This feature article provides a summary of the development of these increasingly popular supramolecular cages based on Ru(II) and Ir(III)

View Article Online
DOI: 10.1039/C8CC08327D

phosphorescent complexes, giving special emphasis to their photophysical properties and their potential in downstream applications. We highlight our contribution to this research area, bringing together our key results while discussing relevant work from other research groups.

Cages based on *d*-block ruthenium(II) and iridium(III) transition metal complexes

Ruthenium cages

Ruthenium(II) polypyridine complexes have enjoyed a rich history in photocatalysis and as redox-active materials.[34] The use of Ru(II) complexes in Dye-Sensitized Solar Cells (DSSC),[35] water splitting,[34b, 36] biological labelling[37] and as anticancer agents[38] is also prominent. However, Ru(II) complexes are generally poorly emissive, their emission energies fall within a narrow range and thus their use as luminophores is limited.[39] Many examples have nevertheless been reported where ruthenium(II) complexes have been incorporated into polymers,[40] metal-organic frameworks[41] and discrete 2-D metallamacrocycles.[42] Recently, examples of 3-D supramolecular cages incorporating Ru(II) complexes as structural components or as metalloligand scaffolds have also been reported. These cage structures are summarized below.

Cook and co-workers[43] recently reported Ru_4L_6-type truncated octahedron, **RuC1**, by assembling the tpt ligand **1** with *cis*-bis(2,2'-bipyridine)ruthenium(II) (Figure **2**).

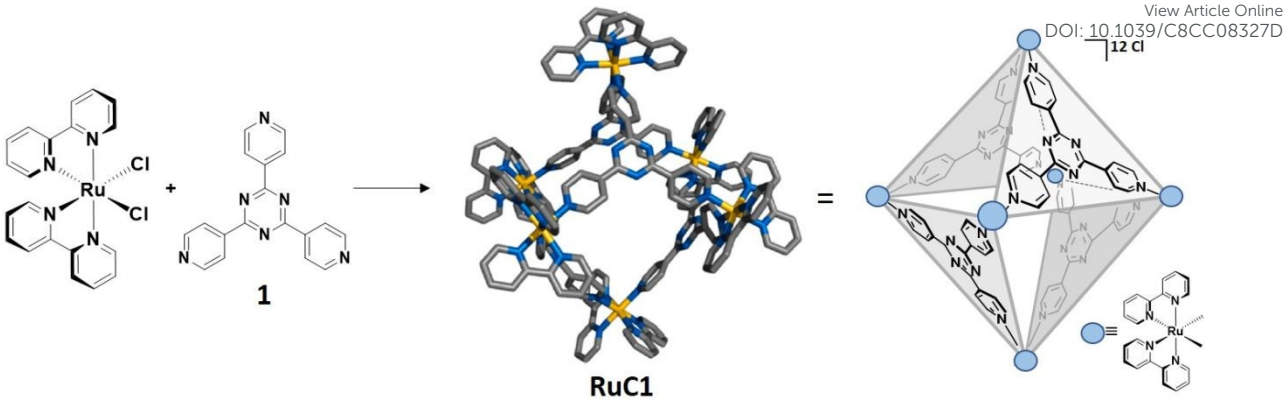

Figure **2**. Coordination driven self-assembly of the tetrahedral cage **RuC1**. The simulated structure of **RuC1** is taken with permission from Ref. [44] Copyright 2018, American Chemical Society.

The photophysical properties of **RuC1** were investigated in MeCN both at room temperature and at 77 K. Cage **RuC1** exhibited a broad emission centred at λ_{PL} = 577 nm at room temperature, with a very low Φ_{PL} < 0.1% and bi-exponential excited state lifetime of τ_{PL} of 2, 790 ns, where the 790 ns component contributes roughly less than 10% to the τ_{PL} of **RuC1**. This emission was red-shifted and strongly quenched compared to the room temperature emission of $[Ru(bpy)_3]Cl_2$ (λ_{PL} = 613 nm, Φ_{PL} = 5%, τ_{PL} = 821 ns).[43] Surprisingly, the 77 K emission of **RuC1** was also red-shifted at λ_{PL} = 689 nm compared to the emission observed at room temperature. Although population of the $^3ML(bpy_{\pi^*})CT$ state was the origin of the room temperature emission of **RuC1**, thermal population of this higher energy excited state no longer occurs at 77 K. Instead, the lower energy $^3ML(TPT_{\pi^*})CT$ was predominantly populated and accounted for the red-shifted emission observed for **RuC1** at 77 K. The electrochemical properties of **RuC1** were investigated by cyclic voltammetry in MeCN. Multiple oxidation waves, corresponding to multiple $Ru^{II/III}$ redox couples were observed, with the first occurring at E^{ox} = 0.56 V (versus $Ag/AgNO_3$), which was significantly cathodically shifted compared to the same redox couple in $[Ru(bpy)_3]Cl_2$ at 1.05 V.[43] The remaining

View Article Online
DOI: 10.1039/C8CC08327D

oxidation waves of **RuC1** ranged from E^{ox} = 0.61 V to 1.08 V. **RuC1** exhibited a single reduction wave at E^{red} = -1.29 V corresponding to the reduction of the bpy ligand, which was anodically shifted compared to the reduction of bpy in $[Ru(bpy)_3]Cl_2$ at -1.64 V. This anodic shift is ostensibly a function of the presence of the electron-poor tpt ligand, which contributes to a reduction of the electron density on the Ru centre. Cage **RuC1** is therefore both a more powerful photoreductant (E_{ox}* = -1.59 V vs -0.97 V) and a more powerful photooxidant (E_{red}* = 0.86 V vs 0.38 V) than $[Ru(bpy)_3]Cl_2$. Stern-Volmer quenching studies were performed to probe the efficiency of **RuC1** as a photoreductant using cobaltocenium hexafluorophosphate as the quencher. However, identical bimolecular rate constants (k_q) of 1.2 x 10^8 s^{-1} were calculated for the electron transfer from both **RuC1** and $[Ru(bpy)_3]Cl_2$ donors to the cobaltocenium hexafluorophosphate acceptor, an indication that the same percentage of effective quenching collisions exists for both chromophores in the presence of cobaltocenium hexafluorophosphate.

A highly symmetric Ru terpyridine-based spherical cage, **RuC2**, was synthetized by Newkome and co-workers[45] via the coordination of four tridentate ligands **2** and six Ru^{2+} ions (Figure **3**).

View Article Online
DOI: 10.1039/C8CC08327D

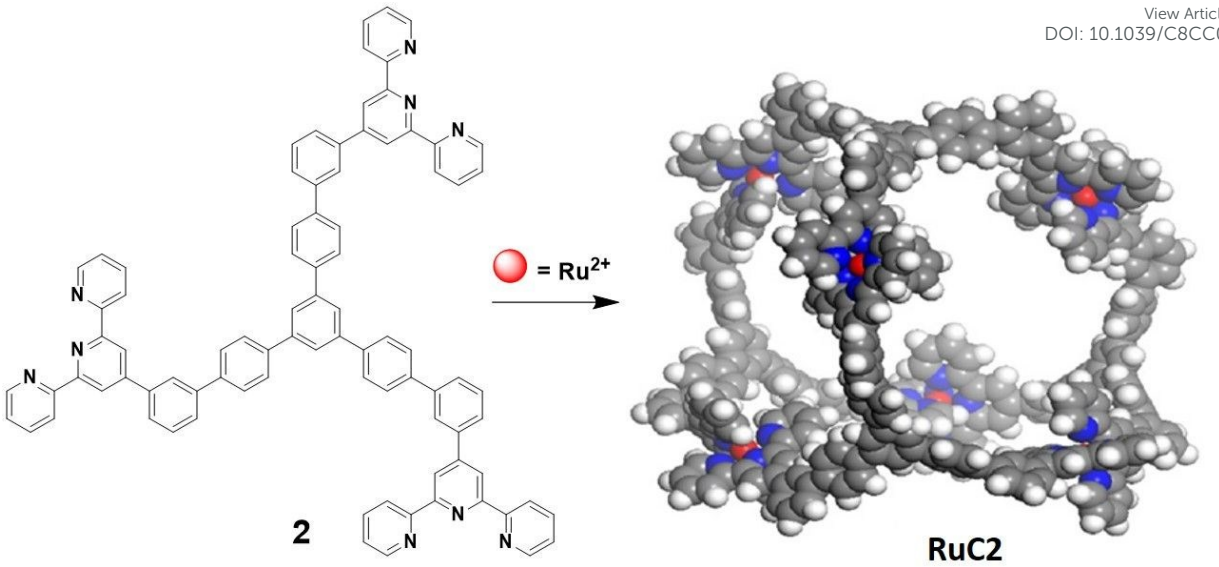

Figure **3**. Chemical structure of ligand **2** and optimised molecular model of cage **RuC2**. Adapted with permission from Ref.[45] Copyright 2014, American Chemical Society.

The geometry of the energy-minimised structure of **RuC2** (Figure **3**) revealed a highly symmetric spherical structure in which the centres of four tridentate ligands **2** form a tetrahedron, and the six Ru^{2+} ions form a regular octahedron of T_d symmetry. The longest distance between two Ru^{2+} centres is 3.2 nm and the inner volume is approximately 4000 $Å^3$. The nanostructure of **RuC2** was probed by Transmission Electron Microscopy (TEM) upon deposition on carbon-coated grids. The size of the nanostructure was found to be ca. 4.1 nm and matched with the diameter obtained for the optimized molecular model of the cage. The emission properties of cage **RuC2** were not investigated.

So far, we have discussed two ruthenium metallocages where the Ru(II) complexes are used as metallic tectons within the supramolecular assembly. However, Ru metalloligands or ligand scaffolds appended with ruthenium complexes have also been used to prepare photophysically- and redox-active supramolecular cages.

View Article Online
DOI: 10.1039/C8CC08327D

A nanosized Pd-Ru heteronuclear metal-organic cage was reported by Su and co-workers.[46] As illustrated in Figure **4a**, the combination of the spatially triangular C_3-symmetric racemic metalloligand ***rac*-Ru1**, bearing three terminal 3-pyridine units, with coplanar spatially square D_4-symmetric naked Pd(II) ions gave rise to the formation of a $[Pd_6(\textbf{\textit{rac}-Ru1})_8]^{28+}$ cage, ***rac*-RuC3**, mediated by $N_{(pyridine)}$-Pd coordination.. Single crystals of ***rac*-RuC3** were obtained by co-crystallizing ***rac*-RuC3** with the heavy coordinating molecule $[Ir(ppy)_2(dc\text{-}bpy)](NO_3)$, $\mathbf{Ir_a}$ (ppy is 2-phenylpyridinato, dc-bpy is 2,2′-bipyridine-4,4′-dicarboxylic acid), yielding red crystals of the composition of $[\textbf{\textit{rac}-RuC3}(\mathbf{Ir_a})_4](NO_3)_{24}$, with the $\mathbf{Ir_a}$ molecules situated outside the structure of cage ***rac*-RuC3**. ***rac*-RuC3** possesses a truncated-octahedral geometry with eight ***rac*-Ru1** metalloligands occupying the eight faces of the cage, six PdN_4 planes truncating the six vertices of the octahedron, and twelve rhombic windows alongside each octahedral edge (Figure **4a**). The dimensions of the cage are 3.1 × 3.4 × 3.4 nm^3, where the six Pd vertices are separated by approximately 29 Å and a large cavity of 5350 $Å^3$ exists. Cage ***rac*-RuC3** was capable of encapsulating neutral non-polar aromatic compounds such as phenanthrene, pyrene and anthracene in a 1:1 mixture of DMSO-d_6/D_2O as a function of the hydrophobic character of its cavity. Molecular dynamic simulations of ***rac*-RuC3** ⊃ phenanthrene revealed that a maximum of seven phenanthrene molecules could reside within the cavity of the cage while an additional seventeen phenanthrene molecules could be accommodated in the "doorway" of twelve cage windows, allowing as many as twenty-four phenanthrene guests to be trapped (Figure **4b**). In addition, ***rac*-RuC3** also exhibited the ability to encapsulate and protect against UV-light radiation three common light-curing agents widely used in inks and paints: 2,2-dimethoxy-2-phenylacetophenone (DMPA), 1-hydroxycyclohexyl phenyl ketone (HCPK) and 2-hydroxy-2-methylpropiophenone (HMPP). While these free molecules photodecomposed upon irradiation at 365 nm for 12 h, no photolysis of the guest molecules was observed after

photoirradiation at 365 nm of ***rac*-RuC3** ⊃ DMPA, ***rac*-RuC3** ⊃ HCPK and ***rac*-RuC3** ⊃ HMPP for 120 h.

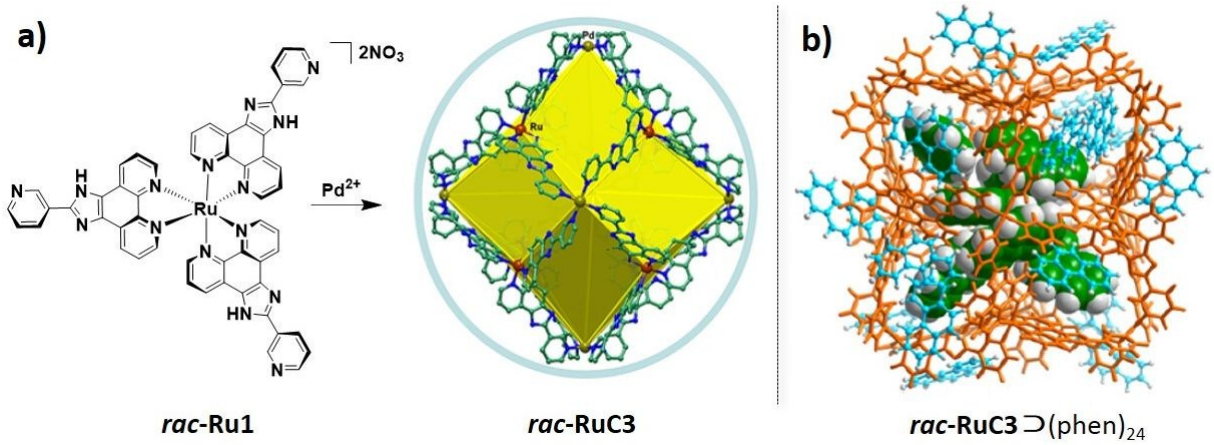

Figure **4**. **a)** Preparation of cage ***rac*-RuC3** from metalloligand ***rac*-Ru1** and Pd(II). The X-ray structure of ***rac*-RuC3** is shown highlighting in yellow its cavity. **b)** molecular dynamics simulation of ***rac*-RuC3** ⊃ phen, showing ***rac*-RuC3** encapsulating phenanthrene guests in its cavity (space-filling mode) and in its windows (stick mode in light blue). Adapted with permission from Ref. [46]. Copyright 2014, American Chemical Society.

Enantiopure metalloligands **Λ-** and **Δ-Ru1** were also prepared in three steps following chiral resolution of *rac*-$[Ru(phen)_3]^{2+}$ with $K_2[Sb_2[(+)\text{-tartrate}]_2]\cdot 3H_2O$, oxidation of Λ- and Δ-$[Ru(phen)_3]^{2+}$ to yield Λ- and Δ-$[Ru(phendione)_3]^{2+}$, which were finally reacted with 3-pyridinecarboxaldehyde in the presence of ammonium acetate in acetic acid.[47] When **Λ-** and **Δ-Ru1** were reacted with Pd^{2+} ions, enantiopure cages of composition Λ_8- and Δ_8-**RuC3** were, respectively, obtained. The enantiopurity and absolute configuration of metalloligands **Λ-, Δ-Ru1** and metallocages **Λ-, Δ-RuC3** were, respectively, confirmed by CD spectroscopy and established by X-ray single crystal analyses. The single crystals of **Λ-** and

Δ-RuC3 were grown from their MeCN solutions in the presence of R-BINOL and S-BINOL, respectively. Both **Λ-** and **Δ-RuC3** crystallized in the chiral space group *I*422 (D_4 symmetry) (Figure **5a**). In **Δ-RuC3**, eight **Δ-Ru1** metalloligands are assembled with six Pd^{2+} ions to form $[Pd_6(\mathbf{Ru1})_8]^{28+}$ with **Ru1** in the *ΔΔΔΔΔΔΔΔ* homochiral configuration, and eight S-BINOL molecules captured in the cage window pockets. Similarly, **Λ-RuC3** integrated eight **Ru1** metalloligands with the *ΛΛΛΛΛΛΛΛ* homochiral configuration and co-crystallised with eight R-BINOL molecules likewise assembled in the cage window pockets. The stereoselective inclusion of chiral molecules of C_2 symmetry such as BINOL, 3-bromo-BINOL, 6-bromo-BINOL and 1,1'-spirobiindane-7,7'-diol, and chiral molecules characterised by a chiral carbon centre such as Naproxen, 1-(1-naphtyl)ethanol and benzoin into the cavity of cages **Λ-** and **Δ-RuC3** were examined by ^{1}H NMR enantiodifferentiation experiments in a 1:5 mixture of DMSO-d_6:D_2O at 298 K. Homochiral cages **Λ-** and **Δ-RuC3** exhibited poor stereoselectivity towards the chiral compounds Naproxen, 1-(1-naphtyl)ethanol and benzoin (encapsulating R- and S-enantiomers with a ratio of ca. 50:50). However, through the same separation process, a pair R- and S-BINOL atropisomers were successfully resolved, with the *ee* values reaching approximately 34% and 36%, respectively, with **Δ-RuC3** (encapsulating R-/S-BINOL with a ratio of 67/33) and **Λ-RuC3** (encapsulating R-/S-BINOL with a ratio of 32/68). Relatively low enantioseparation results were obtained for R- and S-(3-bromo-BINOL) with an *ee* value of approximately 8%. The chiral resolution was greatly improved for the chiral discrimination of R- and S-(6-bromo-BINOL) enantiomers. Indeed, by using **Δ-RuC3** the resolved product contained 77% of the R-isomer and 23% of the S-isomer, giving an *ee* of approximately 54%, while an *ee* of 62% for the S-isomer was obtained by using **Λ-RuC3**. Similarly, **Δ-RuC3** showed preferable

stereoselectivity towards R-(1,1'-spirobiindane-7,7'-diol) with an *ee* value of approximately 34%, while **Λ-RuC3** incorporated primarily the S-isomer with an *ee* value of 44%. In general, **Δ-RuC3** showed a preferable selectivity towards the encapsulation of the R-isomers, while **Λ-RuC3** preferred the encapsulation of the S-isomer for all chiral guests of C_2 symmetry.

In a subsequent work the same group reported the use of the cage ***rac*-RuC3** as a molecular flask to promote cavity-directed photodimerization of 2-naphthol and 3-bromo-2-naphthol, forming racemic mixtures of S- and R-[4-(2-hydroxy-1-naphtyl)-1,2-naphthoquinone] and of its 3-bromo derivative (Figure **5b**).[48] Importantly, when the photodimerization reaction of 3-bromo-2-naphthol was conducted in the cavity of the enantiopure cages **Λ-,** and **Δ-RuC3** (5 mol% loading of cage), an enantiomeric excess of 58% *ee* (product R/S ratio: 79/21) and 54% *ee* (product R/S ratio: 23/77) was, respectively, obtained, albeit in low isolated yields of 9%. Although examples of self-assembled cages as molecular flasks to induce photochemical transformations of encapsulated guests have been previously reported,[16a] with relevant examples involving [2+2] photodimerization of olefins,[49] [2+2] cross-photodimerization,[16d, 50] cyclisation of α-diketones,[51] and photochemical oxidations of alkanes and alkynes,[52] this work showed for the first time that chiral photoactive cages can be used to efficiently promote regio- and enantioselective photo-transformations of bound guests.

View Article Online
DOI: 10.1039/C8CC08327D

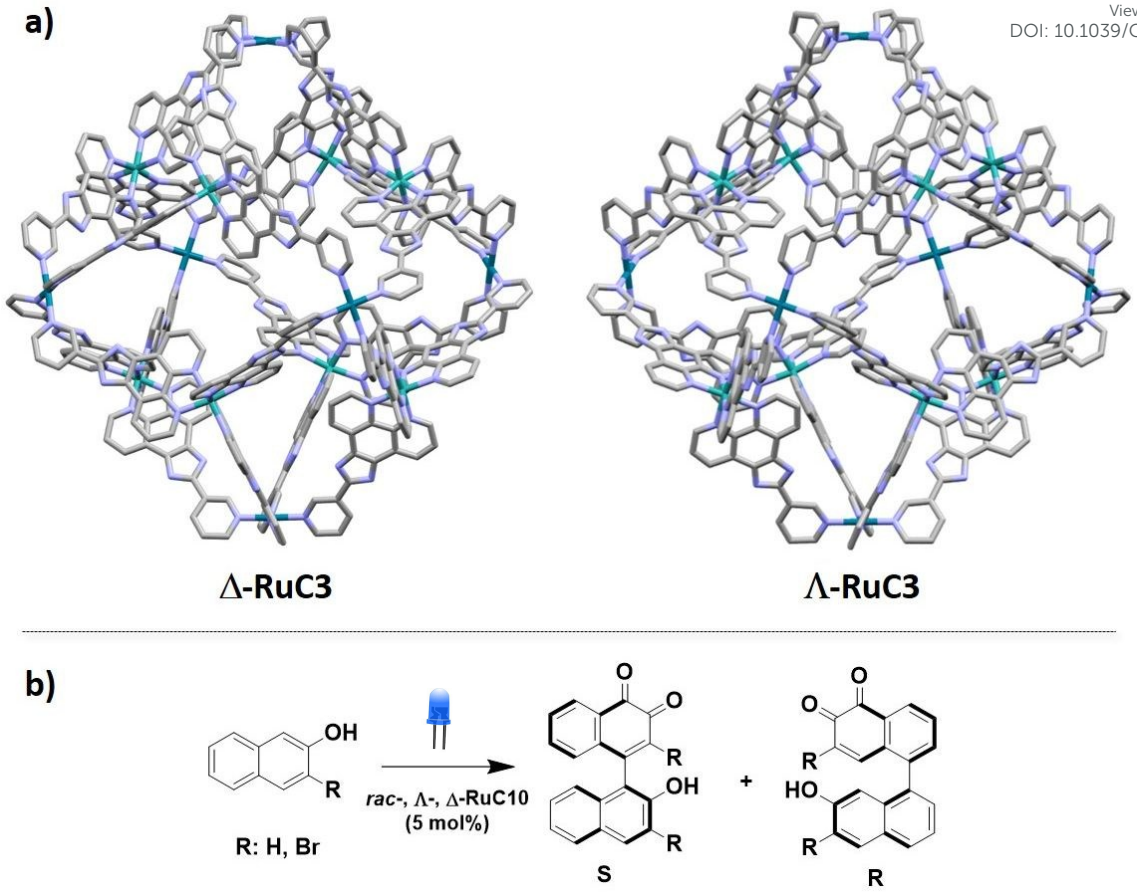

Figure **5**. **a)** X-ray structure of enantiopure cage **Δ-RuC3** (left) and **Λ-RuC3** (right). The blue sphere illustrates the cavity of the cage. **b)** photoinduced dimerization of 2-naphtol and 3-bromo-2-naphtol in the presence of cage ***rac-*, Λ-** and **Δ-RuC3**. The system was irradiated with 8W blue LED light (λ_{exc} = 453 nm) in air in MeCN:H_2O = 1:1.

During the last decade, research into solar fuels has greatly accelerated, mostly in the area photocatalytic water splitting to generate cleanly hydrogen gas.[34b] Remarkable progress has been made since the development of intramolecular photochemical molecular devices (PMDs) by integrating chromophoric photosensitizers, catalytic centers and electron relay components into a single photocatalyst.[53] For example, many photoactive multimetallic PMDs[36a] have been

developed as photocatalysts for hydrogen production including: trinuclear Ru-Pt$_2$,[54] Ru-Pt$_2$,[55] and Ru-Rh-Ru;[56] or tetranuclear Ru$_2$-Ru-Pt;[57] and Ru-Pt$_3$[55] complexes. The best examples of these have achieved up to 870 turn-over numbers (TON) after 46 h.[56] Cage ***rac*-RuC3** is a highly organized structure that is composed of eight Ru^{2+} photocenters connected to six catalytically active Pd^{2+} centers through a phenanthroline (phen) bridging ligand and a benzimidazole-pyridine (biim-py) peripheral unit. Importantly, this system mimics the composition of PMDs (Figure **6**).[58]

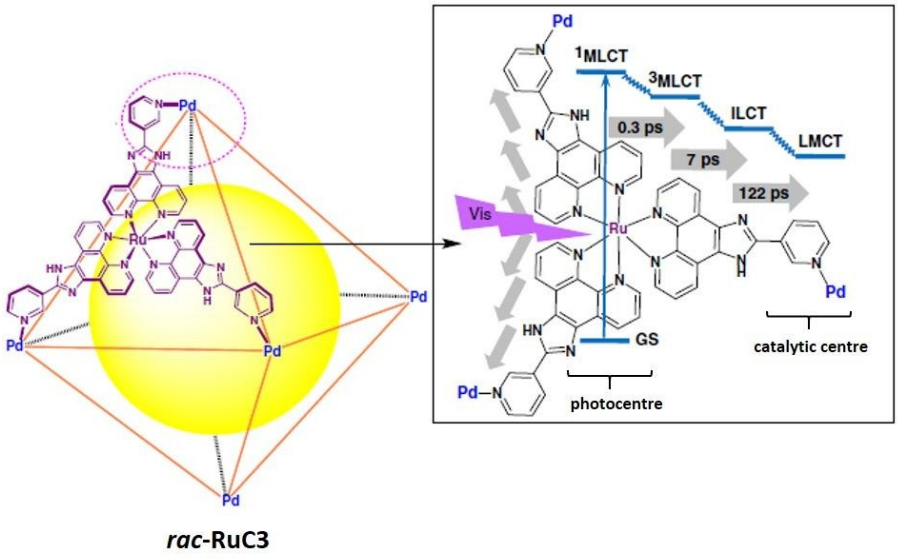

Figure **6**. Representation of the octahedral cage structure of ***rac*-RuC3** and the multi-channel electron transfer pathways between chromophoric Ru and catalytic Pd metal centers. GS: ground state; ILCT: intraligand charge transfer; LMCT: ligand-to-metal charge transfer; MLCT: metal-to-ligand charge transfer. Adapted from Ref. [58]. Published by Springer Nature.

The metalloligand ***rac*-Ru1** and cage ***rac*-RuC3** showed similar emission spectra with maxima at ca. 610 nm, which correspond for both ***rac*-Ru1** and ***rac*-RuC3** to the emission from Ru(phen)$_3$-centred triplet ^{3}MLCT states. However, compared to that of ***rac*-Ru1**, the emission

intensity of ***rac*-RuC3** was reduced by ca. 32% due to intramolecular charge transfer from $Ru(phen)_3$ to the $Pd(pyridine)_4$ moieties. Both DFT calculations and ultrafast transient absorption spectroscopy were employed to elucidate the electronic structure of ***rac*-RuC3**. The photoexcitation of the $[Ru(phen)_3]^{2+}$ chromophore at 400 nm populates the ^{1}MLCT state, which is rapidly followed by intersystem crossing (ISC) to populate the ^{3}MLCT state involving the phenanthroline. The subsequent excited state relaxation occurs via an intraligand charge transfer (ILCT) process from phen to biim-py, and finally, a much slower process of ligand-to-metal charge transfer (LMCT) takes place from biim-py to the Pd catalytic center (Figure **6**). The photocatalytic hydrogen production exhibited by cage ***rac*-RuC3** in a closed gas circulation and evacuation system upon irradiation with visible light ($\lambda_{exc} > 420$ nm) was found to be efficient. Indeed, under optimised conditions (100 mL DMSO solution with 22 μM ***rac*-RuC3**, 0.34 M H_2O and 0.75 M triethanolamine), the reaction rate for H_2 production was found to be 380 μmol·h^{-1} with a turnover number of 635 after 48 h. The efficiency of H_2 production by using ***rac*-RuC3** as a photocatalyst is comparable to those observed for H_2 production with photoactive multimetallic PMDs.[36a]

Beves and co-workers[59] designed the Ru(II) complexes **Ru2** and **Ru3** featuring a $[Ru(tpy)_2]^{2+}$ core (tpy is 2,2′,6′,2″-terpyridine) decorated at the 4′-position with a 3,5-disubstited benzene containing 4-pyridyl groups capable of coordinating to square-planar Pd metal centres (Figure **7**). Reaction of **Ru2** with two equivalents of $[Pd(dppp)](OTf)_2$ (dppp is 1,3-diphenylphosphinopropane) in nitromethane at room temperature immediately afforded a single major species in solution, the composition and purity of which were ascertained to be $[(Pd(dppp))_8(\mathbf{Ru2})_4](PF_6)_{24}$ (**RuC4** in Figure **7a**) by ESI-mass spectrometry and ^{1}H- and ^{31}P-NMR spectroscopy. The analogous reaction of complex **Ru3**, which features alkyne spacers

between the phenyl and pendant pyridyl rings, and [Pd(dppp)](OTf)$_2$ gave rise to a trimeric rather than a tetrameric structure as observed for the assembly of **Ru2**, of the composition of [(Pd(dppp))$_6$(**Ru3**)$_3$](PF$_6$)$_{18}$ (**RuC5** in Figure **7b**). The simulated structure of **RuC5** is illustrated in Figure **7b**. **RuC4** crystallized in the $P\bar{1}$ space group and exhibits a box-like structure of dimensions of ca. 21 × 21 × 32 Å, with Pd(II) centers located at each end of the box forming almost perfect squares (Pd-Pd-Pd angles of 86.0˚-92.8˚ and Pd···Pd distances of 13.2-13.4 Å). The center of the cage is occupied by [Ru(tpy)$_2$] units with alternating Ru···Ru distances of 11.82 Å and 8.78 Å. Preliminary investigation of the photophysical properties of **RuC5** and **RuC6** revealed that their emissions are similar to those of the corresponding metalloligands **Ru2** and **Ru3**. All the species exhibited weak emissions at λ_{PL} = 640 nm from ^{3}MLCT states centered on the [Ru(tpy)$_2$] chromophores with very short mono-exponential excited state lifetimes of 1.59 ns, 2.04 ns, 1.95 ns and 2.53 ns, respectively, for **Ru2**, **RuC4**, **Ru3** and **RuC5**. The photophysical properties of **Ru2**, **RuC4**, **Ru3** and **RuC5** are also comparable to those previously reported for the related [Ru(4′-tolyl-tpy)(bis-tpy)]$^{2+}$ complex (tolyl-tpy is 4′-(*p*-tolyl)-2,2′;6′,2″-terpyridine, bis-tpy is 1,4-di-[(2,2′;6′,2″-terpyridin)-4′-yl]benzene.[60]

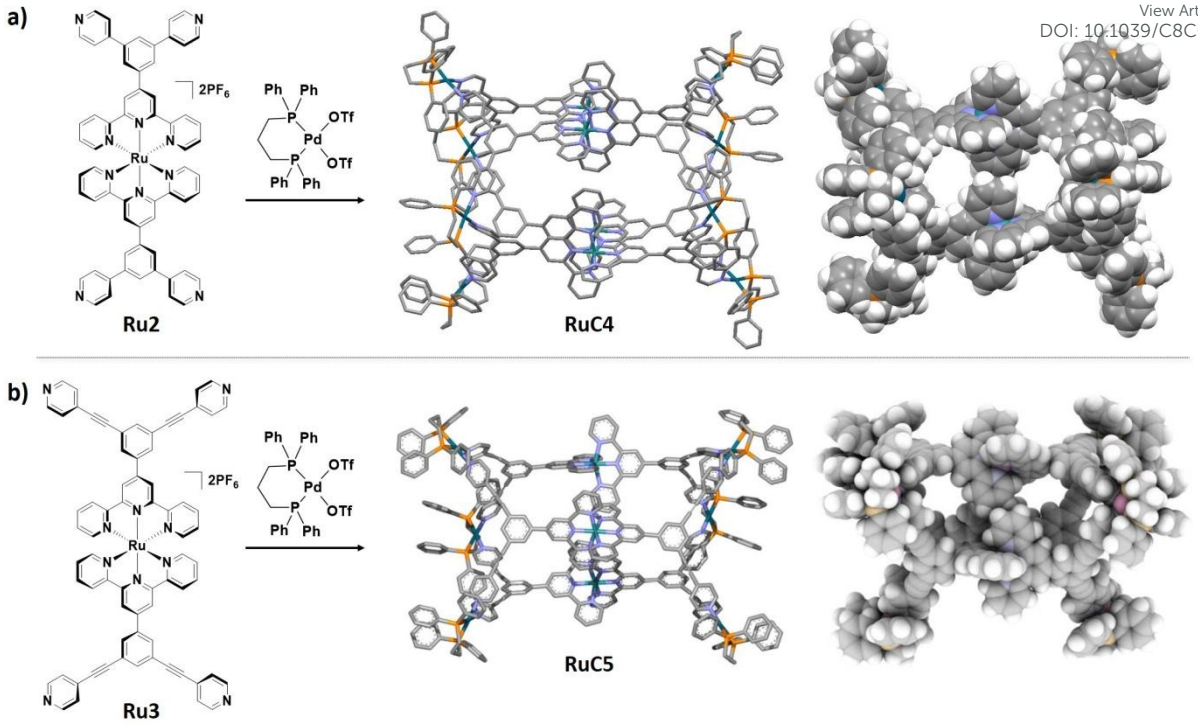

Figure **7**. **a)** Self-assembly between the Ru metalloligand **Ru2** and [Pd(dppp)](OTf)$_2$ to yield cage **RuC4**. The X-ray structure of **RuC4** is illustrated in capped sticks (left) and spacefill (right) modes. **b)** Self-assembly between the Ru metalloligand **Ru3** and [Pd(dppp)](OTf)$_2$ to yield cage **RuC5**. The simulated structure of **RuC5** is taken from Ref [59] – Published by the Royal Society of Chemistry.

More recently, the same group synthetized four dinuclear ruthenium(II) terpyridine complexes appended with terminal 3- and 4-pyridyl groups.[61] However, among this series of complexes only the reaction between the dimeric complex **Ru4** (Figure **8**) and [Pd(NCMe$_4$)](BF$_4$)$_2$ (0.6 equiv.) in MeCN-d_3 gave an identifiable clean product, **RuC6**, rather than polymeric structures as observed for the other three complexes. The composition of the assembled structure **RuC6** was identified by ESI-mass spectrometry as [Pd$_2$(**Ru4**)$_4$]$^{20+}$. As illustrated in Figure **8**, the simulated geometry of **RuC6** resembles a cage-like structure with a distance between the Ru(II) centres within the same dinuclear metalloligand of approximately 13 Å. The size of the simulated structure of **RuC6** is in good agreement with the measured

diffusion data obtained by ^{1}H DOSY NMR spectroscopy (hydrodynamic radius, r_s = 2 nm). **RuC6** was, however, noted to not be emissive.

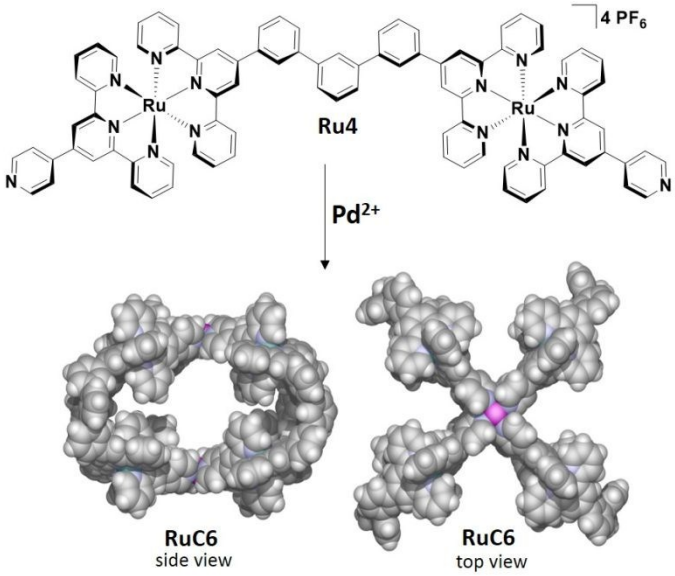

Figure **8**. Self-assembly between the Ru metalloligand **Ru4** and Pd^{2+} ions to yield cage **RuC6**. The molecular mechanics model (Spartan 14) of cage **RuC6** is illustrated showing the enclosed cavity (left) and the 4-fold symmetry along the Pd-Pd axis (right).[61]

Our group has recently reported a phosphorescent cage of the form of $[Pd_4Ru_8]^{24+}$, **RuC7**, which was formed by assembling the metalloligand $[Ru(dtbubpy)_2(qpy)]^{2+}$, **Ru5**, where qpy is 4,4':2',2":4",4"'-quaterpyridine and *dt*bubpy is 4,4'-di-*tert*-butyl-2,2'-bipyridine, with Pd^{2+} ions (Figure **9a**).[62] X-ray diffraction analysis revealed that cage **RuC7** is constructed such that two **Ru5** ligands doubly bridge adjacent Pd(II) centres in a crown-like fashion disposing the four palladium ions in a square arrangement. **RuC7** has a diagonal distance of 38.4 Å and an internal volume of 4900 Å^3 which makes it the largest X-ray structure reported to date of a Ru(II) cage assembled with Pd^{2+} ions.

View Article Online
DOI: 10.1039/C8CC08327D

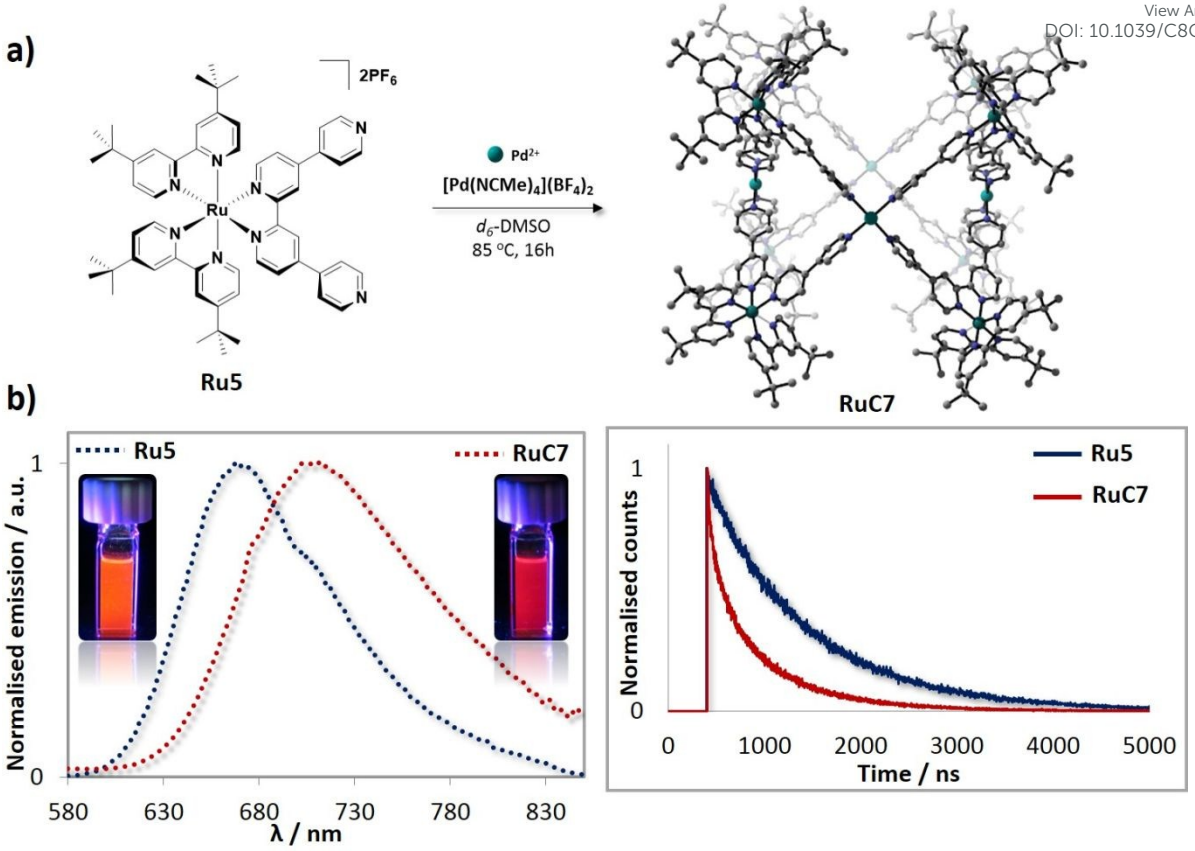

Figure **9**. **a)** Self-assembly between **Ru5** and Pd^{2+} ions yielding the cage **RuC7,** showing the X-ray structure. **b)** Left: normalized emission spectra of **Ru5** (dotted blue line) and **RuC7** (dotted red line) in degassed DCM at 298 K (λ_{exc} = 360 nm). Photographs of the emissions of **Ru5** (left) and **RuC7** (right) in DCM are inset to the spectra. Right: emission decays of **Ru5** (blue line) and **RuC7** (red line) in degassed DCM at 298 K (λ_{exc} = 378 nm). Adapted from Ref [62] – Published by the Royal Society of Chemistry.

The near-infrared emission exhibited by **RuC7** in DCM (λ_{PL} = 710 nm) is broader and red-shifted compared to that of **Ru5** (λ_{PL} = 674 nm, Φ_{PL} = 7.3%), and with a photoluminescence quantum yield of 6.9% (Figure **9b**). Notably, the Φ_{PL} of **RuC7** is one of the highest reported among ruthenium cages and it is remarkably high considering its emission at 710 nm. The red-shifted emission of **RuC7** compared to **Ru5** is the result of the coordination of the Lewis acidic Pd(II) ions to the ruthenium complex, which essentially stabilises the π^*_{qpy} orbital levels

involved in the emission, and thus lowers the energy of the triplet state. Both **RuC7** and **Ru5** exhibit bi-exponential photoluminescence decay kinetics with τ_{PL} of 324, 1047 ns and 151, 700 ns, respectively (Figure **9b**). As a result, similar radiative rate constants, k_r, of 6.97×10^4 s^{-1} and 9.86×10^4 s^{-1}, and non-radiative rate constants, k_{nr}, of 8.85×10^5 s^{-1} and 13.30×10^5 s^{-1} are obtained for **RuC7** and **Ru5**, respectively. Thus, the Pd(II) ions in **RuC7** do not adversely affect the photophysical properties of **Ru5**. This observation is rather unusual considering that the emissions of the vast majority of metal complexes assembled within cage structures, including those of **RuC3**, **RuC4**, **RuC5** and **RuC6**, are often partially or fully quenched by the presence of Pd(II) ions due to the population of low-lying dark states involving the donor and Pd(II) acceptor units. The fact that, in this specific case, the photoluminescence of **Ru5** is not quenched in the cage indicates that the radiative process in **RuC7** is sufficiently fast to compete with internal conversion to the lower-lying dark states.

Beves, Moore and co-workers[63] have recently designed linear Ru(II) metalloligands that contain a central photoactive $[Ru(phen)_2(bpy)]^{2+}$ structure with the bpy unit functionalized at the 5 and 5′ positions with peripheral metal binding sites such as 2,2'-bipyridine (in **Ru6**) or picolinaldehyde (in **Ru7**), Figure **10**. When metalloligand **Ru6** was self-assembled with Fe(II) ions, the tetrahedral cage **RuC8** was formed (Figure **10a**), while the condensation reaction between **Ru7** and the capping ligand tris(2-aminoethyl)amine in the presence of Zn(II) ions gave rise to the tetrahedral cage **RuC9** (Figure **10b**). In MeCN, cages **RuC8** and **RuC9** exhibited weak emissions at 640 nm and 660 nm, respectively, which were at the same energy as those of their respective parent metalloligands **Ru6** and **Ru7**. Unfortunately, the Φ_{PL} and τ_{PL} values of the complexes were not reported.

View Article Online
DOI: 10.1039/C8CC08327D

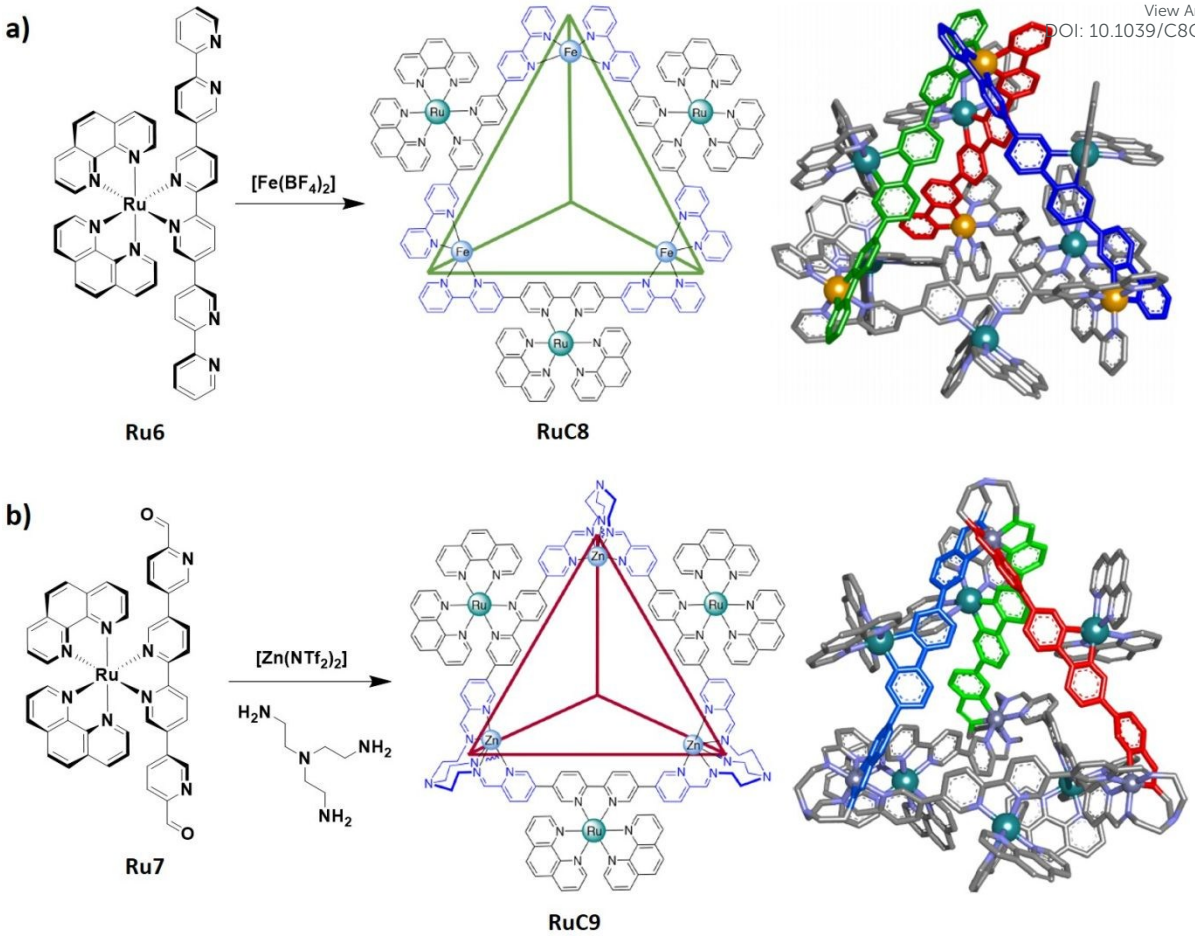

Figure **10**. Synthesis and molecular model of **a)** cage **RuC8** and **b)** cage **RuC9**. Adapted with permission from Ref. [63]. Copyright 2016, American Chemical Society.

Metallosupramolecular 3D assemblies of heterodimetallic Zn_4(**Ru8**)$_2$ (**RuC10**), and heterotrimetallic Fe_2Zn_2(**Ru8**)$_2$ (**RuC11**) were recently reported by Newkome, Wang and co-workers (Figure **11**).[64] As illustrated in Figure **11a**, **RuC10** was prepared by assembling the ruthenium metalloligand **Ru8** (1 equiv.), possessing four uncomplexed terpyridine units, with $Zn(NO_3)_2{\cdot}6H_2O$ (2 equiv.). When **Ru8** was treated with one equivalent of $FeCl_2{\cdot}4H_2O$, it spontaneously generated the dimeric stable intermediate **Ru9** (Figure **11b**), which was then reacted with one equivalent of $Zn(NO_3)_2{\cdot}6H_2O$ to obtain the trimetallic **RuC11** supramolecule.

There is, however, no comment on the photophysical properties of these assemblies despite the presence of photoactive but poorly emissive bis(terpyridyl) Ru metalloligands.

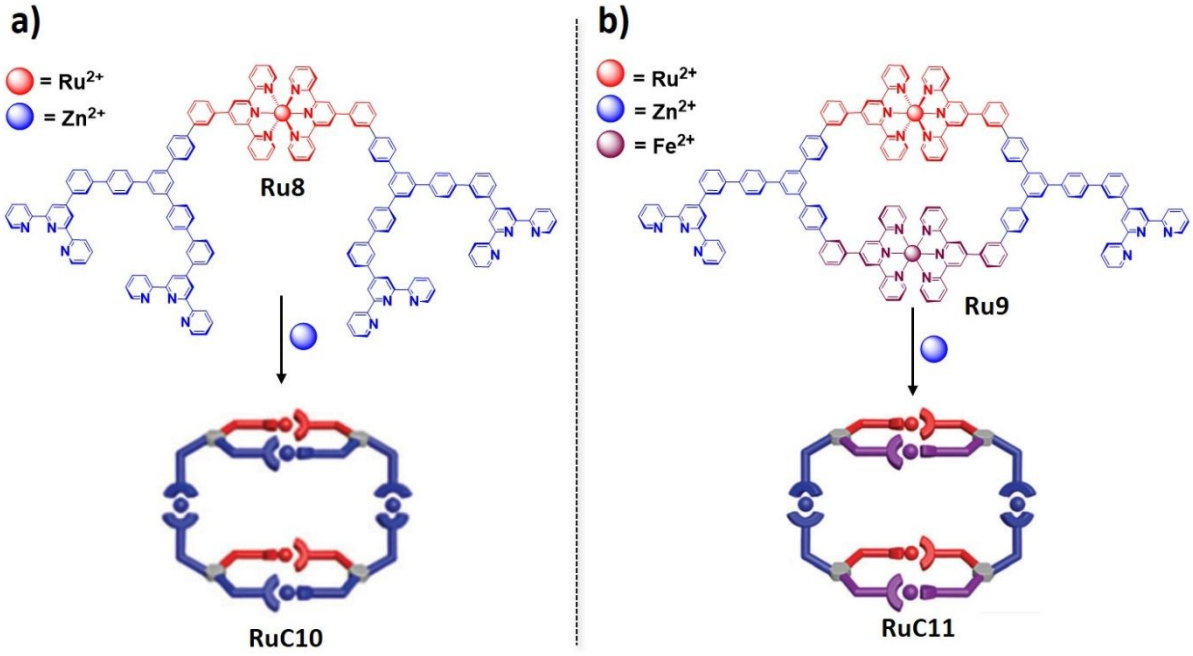

Figure **11**. Illustration of the self-assembly of: **a)** dimetallic **RuC10** from **Ru8** and **b)** trimetallic **RuC11** from **Ru9**. Ref [64] – Published by the Royal Society of Chemistry.

Ward and co-workers[65] reported a heterometallic cage of composition $[Ru_4Cd_4L_{12}](ClO_4)_{16}$, **RuC12**, Figure **12**, (L is the pyrazolyl-pyridine ligand shown in Figure **12)** by reacting the metalloligand $[RuL_3](PF_6)_2$, **Ru10**, with $Cd(ClO4)_2$. Both **Ru10** and **RuC12** exhibited a single reversible Ru^{2+}/Ru^{3+} oxidation wave respectively at +0.85 V and +0.96 V. The presence of the Cd ions in **RuC12** partially removes electron density from the Ru(II) centres and therefore the oxidation of **RuC12** resulted shifted at a higher potential when compared to that of **Ru9**. The emission properties of **Ru10** and **RuC12** were not discussed.

View Article Online
DOI: 10.1039/C8CC08327D

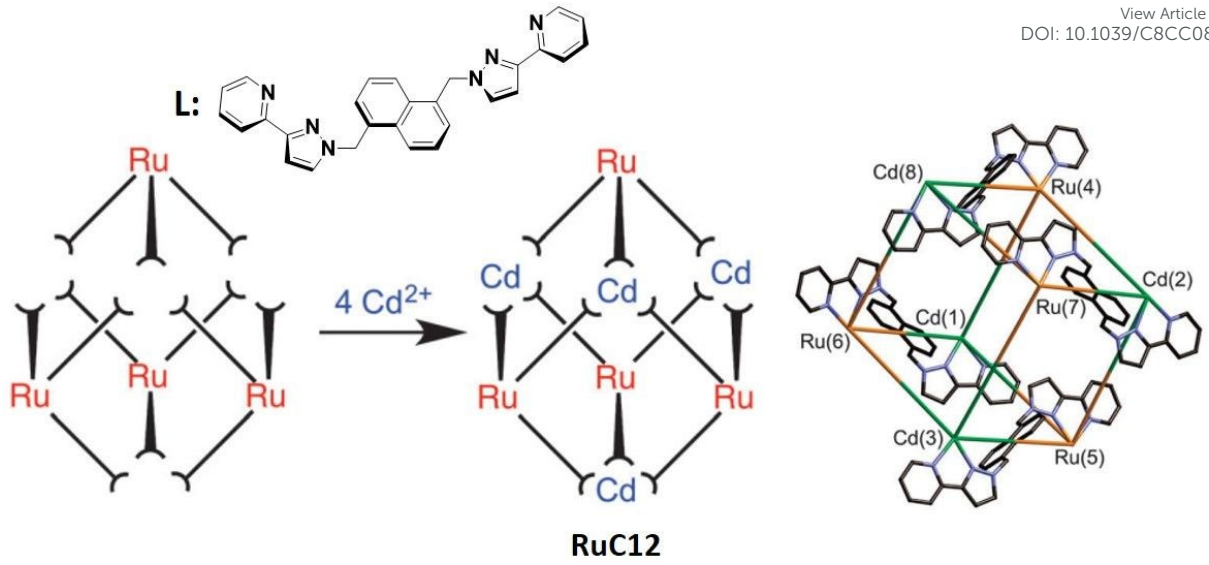

Figure **12**. Schematic diagram of the reaction between four **Ru10** complexes and four Cd^{2+} ions to form cage **RuC12**. The X-ray structure of **RuC12** is shown. Adapted with permission from Ref [65] – Published by the Royal Society of Chemistry.

As exemplified by cages **RuC3**, **RuC4**, **RuC5** and **RuC6**, the emissions of Ru metalloligands often are partially or completely quenched when the Ru complexes are situated in a close proximity to Pd^{2+} ions, which is due to the formation of non-emissive charge-transfer states involving the ruthenium and the palladium centres. This problem can be avoided by electronically isolating the emissive Ru(II) metal complexes from the Pd(II) metal ions. In this context, there have been reports of functionalized cages generated from ligands appended at their exohedral[66] or endohedral[67] faces with photoactive complexes. Additionally, there have been only a few examples reported wherein the photoactive complex is installed via post-synthetic modification of the inert metallo-supramolecular species.[68]

Crowley, Gordon and co-workers recently reported $[Pd_2L_4]^{4+}$ metallo-supramolecular cages constructed from a tripyridyl-1,2,3-triazole backbone *exo*-functionalized with Ru(II) complexes.[67b] In particular, they used copper(I)-catalysed azide-alkyne cycloaddition (CuAAC) "click" reactions[66c] to append the chromophoric moieties $[Ru(bpy)_2(az\text{-}py)](PF_6)_2$, **Ru11**, and $[Ru(bpy)_2(az\text{-}bpy)](PF_6)_2$, **Ru12**, (bpy is 2,2′-bipyridine, az-py is 3-(1-methyl-1*H*-1,2,3-trazol-4-yl)pyridine and az-bpy is 5-(1-methyl-1*H*-1,2,3-triazol-4-yl)-2,2′-bipyridine) to the concave bipyridine ligand scaffold used to form the *exo*-functionalized Pd_2L_4 cages (Figure **13**).

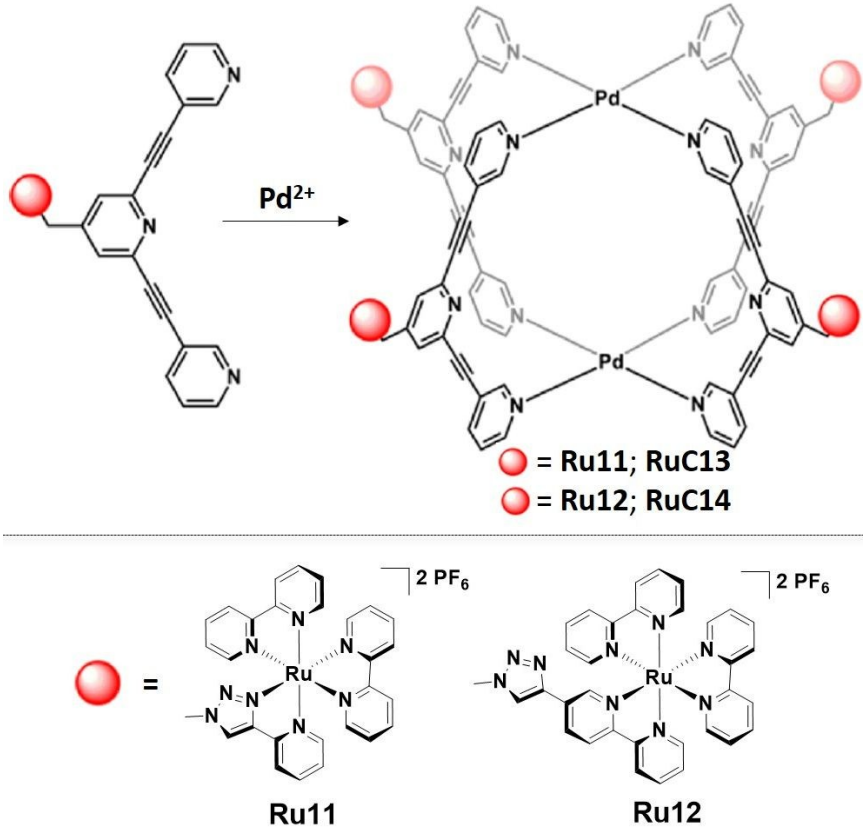

Figure **13**. Chemical structure of the Ru chromophores **Ru11** and **Ru12** appended to the Pd_2L_4 cages **RuC13** and **RuC14**. Adapted with permission from Ref. [67b]. Copyright 2016, American Chemical Society.

View Article Online
DOI: 10.1039/C8CC08327D

Cages **RuC13** and **RuC14** were prepared in good yield (> 70%) by simply stirring metalloligands **Ru11** and **Ru12** with $[Pd(NCMe)_4](BF_4)_2$ in MeCN (Figure **13**). In degassed DMF at room temperature **RuC13** and **RuC14** exhibited ruthenium-based ^{3}MLCT emissions centred, respectively, at 620 nm and 638 nm, with Φ_{PL} of 0.2% and 2.6% and τ_{PL} of 20 ns and 659 ns, respectively. The ruthenium complexes **Ru11** and **Ru12** exhibited identical emission maxima compared to the corresponding metallocages **RuC13** and **RuC14** and similar Φ_{PL} of 0.2% and 6.5% and τ_{PL} of 21 ns and 943 ns, respectively. These results indicate that the Pd_2L_4 cage and the ruthenium chromophores in **RuC13** and **RuC14** are electronically isolated. Electrochemical investigation also revealed minimal perturbation of the ground state redox properties of the Ru chromophores **Ru11** and **Ru12** when incorporated into **RuC13** and **RuC14**. Cyclic voltammetry (CV) and differential pulse voltammetry (DPV) measurements carried out in degassed DMF evidenced four consecutive quasi-reversible reduction processes for both **Ru11** and **Ru12**. The electrochemistry of **Ru11** closely resembled that of the structurally similar $[Ru(bpy)_2(pytri\text{-}Bn)]^{2+}$ complex[69] (pytri-Bn is 2-(1-benzyl-1*H*-1,2,3-triazol-4-yl)pyridine), with the first two reduction processes at $E^{red} = -1.28$ V and $E^{red} = -1.36$ V associated with the bpy ligands and the remaining two reductions at $E^{red} = -1.64$ V and $E^{red} = -1.80$ localized on the pytri-Bn ligand. Similarly, the first three reductions of **Ru11** at $E^{red} = -1.17$ V, $E^{red} = -1.39$ V and $E^{red} = -1.65$ V were assigned the reductions of the bpy ligands and matched with the potentials for the reductions of bpy in $[Ru(bpy)_3](PF_6)_2$ in DMF.[69] The forth reduction process of **Ru12** at $E^{red} = -1.80$ V was attributed to the reduction of the bis-triazole ligand.[70] For both **Ru11** and **Ru12** a chemically reversible $Ru^{II/III}$ oxidation was observed at $E^{ox}_{1/2} = 1.31$ V and $E^{ox}_{1/2} = 1.32$ V, respectively. The electrochemical behavior of **RuC13** and **RuC14** mirror those of the respective complexes **Ru11** and **Ru12** (For **RuC13**: $E^{red} = -1.27$ V, 1.36 V, 1.64 V and 1.80 V; $E^{ox}_{1/2} = 1.33$ V; For **RuC14**: $E^{red} = -1.18$ V, 1.40 V, 1.69 V and 1.80 V; $E^{ox}_{1/2} = 1.31$ V). DFT calculations and Raman spectroscopy further confirmed minimal

electronic communication between the Pd_2L_4 cage unit and the *exo*-appended Ru(II) chromophores. As a result, the *exo*-functionalization of metallo-supramolecular cages opens the possibility of aggregating photophysically and redox active moieties, via cage assembly, without compromising their photophysical properties.

Casini, Kuhn and co-workers[71] also reported Pd_2L_4 cages *exo*-functionalized with Ru(II) pyridine complexes via coordination-driven self-assembly. They coupled two Ru(II) complexes of the composition of $[Ru(tpy)(tpy\text{-}4\text{-}CO_2H)](PF_6)_2$ and $[Ru(bpy)_2(bpy\text{-}alk\text{-}CO_2H)](PF_6)_2$ (tpy is 2,2';6',2"-terpyridine; tpy-4-CO_2H is 2,2';6',2"-terpyridine-4'-carboxylic acid and bpy-alk-CO_2H is 3-(4-methyl-[2,2'-bipyridin]-4-yl)propanoic acid) with the amine-based ligand scaffold 3,5-bis(pirydin-3-ylethynyl)aniline using 2-chloro-1-methyl pyridinium iodide (CMPI) as the coupling reagent and DMAP as the base, forming complexes **Ru13** and **Ru14** (Figure **14**).

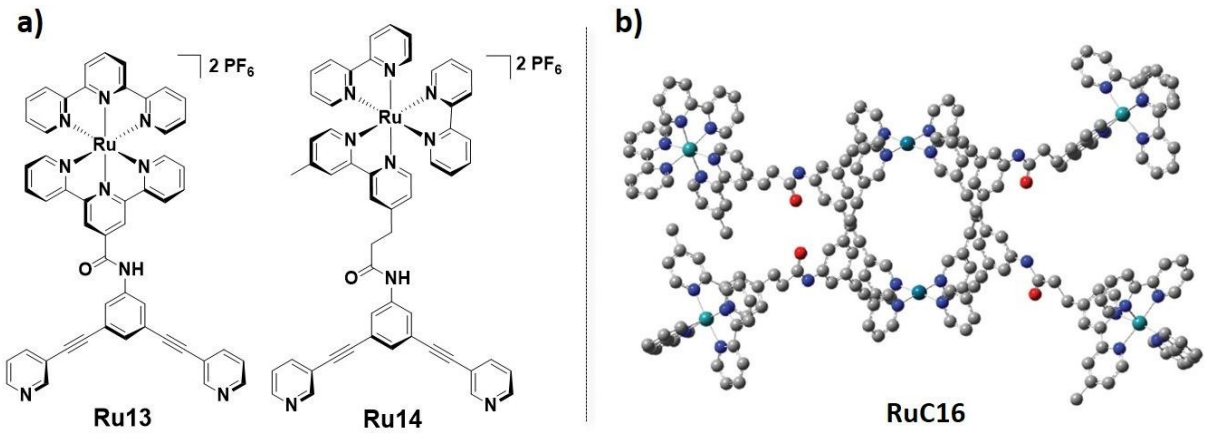

Figure **14**. **a)** chemical structures of Ru-appended metalloligands **Ru13** and **Ru14**. **b)** molecular model of cage **RuC16** (C grey, N blue, O red, Pd turquoise, Ru green). Image **b)** is adapted from Ref. [71] – Published by The Royal Society of Chemistry.

The coordination cages **RuC15** and **RuC16** of the composition of $[Pd_2(\mathbf{Ru13})_4]^{12+}$ and $[Pd_2(\mathbf{Ru14})_4]^{12+}$ were assembled by mixing the respective Ru metalloligands **Ru13** and **Ru14** with $[Pd(NCMe)_4](BF_4)_2$ in DMSO at room temperature for one hour. The optimised structure, obtained from semi-empirical calculations, of **RuC16** exhibited a Pd···Pd distances of 1.1 nm, a distance between the opposing inner C-atoms of 1.2 nm and a span of 5.0 nm. The metallocages **RuC15** and **RuC16** showed distinct emissive properties, demonstrating that the luminescence of the cages is either increased or decreased by altering the molecular structure of the ligand framework. The complex **Ru13** and the corresponding cage **RuC15** are not emissive. However, upon irradiation of metalloligand **Ru14** and cage **RuC16** at 260 nm, strong orange phosphorescence at λ_{PL} = 640 nm were observed with unusually high Φ_{PL} values for Ru-based luminophores of 88% and 66%, respectively, for **Ru14** and cage **RuC16**. These results demonstrated that the electronic separation of the Ru-based chromophores from the coordinating bis(pyridyl) ligand using an alkyl spacer can give rise to the formation of highly emissive ruthenium cages. To the best of our knowledge **RuC16** exhibited one of the highest Φ_{PL} reported for supramolecular coordination cages. However, such an unprecedentedly high Φ_{PL} value contrasts with the those reported for analogous ruthenium(II) complexes, which generally exhibit Φ_{PL} values below 20%.[39a]

In summary, cage compounds incorporating ruthenium complexes generally maintain the redox properties associated with the ruthenium chromophores. We have described that ruthenium cages can act both as photooxidants and photoreductants and can be efficiently used as photocatalysts for hydrogen production and in chemical reactions. As exemplified by cage **RuC3**, the cavity of cage compounds coupled with the intrinsic chirality and photoactivity of ruthenium complexes make ruthenium cages very interesting photocatalysts that can

encapsulate guest compounds and promote their transformations in enantioselective fashions. On the other hand, the emission properties of ruthenium cages are not very tunable and fall within a narrow range in the red/deep-red region of the visible spectrum, similar to their metalloligands. As a result, the use of ruthenium assemblies as light-emitting materials remains very limited.

Iridium capsules and cages

Cyclometalated iridium(III) complexes exhibit efficient phosphorescence, have a capacity to have their emission energy modulated across the visible spectrum, and show high chemical and thermal stability.[72] They have been employed within many applications such as in sensing,[73] bio-imaging,[74] photoredox catalysis,[75] solar fuels[76] and in electroluminescent devices.[77] The use of iridium complexes as luminescent components in discrete cage-like structure has recently become increasingly popular.[78] In this section we comprehensively summarize the preparation and the optoelectronic properties of photoactive Ir(III) capsules and cages.

The first example of a 3D luminescent Ir(III) octahedral capsule, **IrC1**, of composition of $[(Ir(ppy)_2)_6(tcb)_4](OTf)_6$ (tbc is 1,3,5-tricyanobenzene), Figure **15**, was reported Lusby and co-workers.[79] Firstly the racemic *rac*-$[Ir(ppy)_2Cl]_2$ was resolved into its enantiopure Λ,Λ- and Δ,Δ-stereoisomers through chromatographic resolution of serine-based complexes, the amino acid acting as a chiral ancillary ligand. The subsequent treatment of Λ,Λ- and Δ,Δ-$[Ir(ppy)_2Cl]_2$ with tcb quantitatively yielded the enantiopure capsules Λ_6- and Δ_6-**IrC1**. The racemic and enantiopure capsules were characterized by ^1H, ^{19}F NMR and CD spectroscopies and ESI-mass spectrometry. In addition, the geometry of the enantiopure Δ_6-**IrC1** capsule was

View Article Online
DOI: 10.1039/C8CC08327D

elucidated by single crystal X-ray diffraction. The solid-state structure supports the solution structure, $[(Ir(ppy)_2)_6(tcb)_4](OTf)_6$, which is a truncated octahedron with triflate anions located in each of the octahedron windows. Compared to the bis(benzonitrile) reference complex $[Ir(ppy)_2(NCPh)_2]OTf$, which exhibited a weak emission ($\Phi_{PL} < 1\%$) at λ_{PL} = 525 nm in deaerated tetrachloroethane, the emission of capsule **IrC1** in the same solvent was broad and red-shifted at 575 nm, with an unusually enhanced Φ_{PL} of 4%.

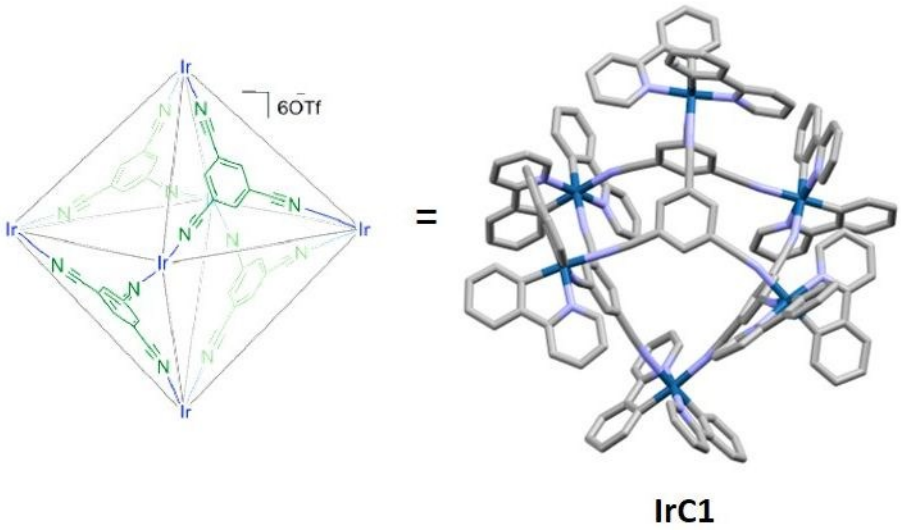

Figure **15**. X-ray crystal structures of **IrC1**. Solvent molecules and counterions are omitted for clarity. The octahedron is adapted with permission from Ref.[79]. Copyright 2012, American Chemical Society.

Duan and co-workers reported the multicomponent self-assembly of two pentanuclear Ir(III)-Zn(II) (**IrC2**)[80] and Ir(III)-Co(II)[81] (**IrC3**) heterometallic polyhedral capsules via imine bond formation. Polyhedron **IrC2** was obtained by reacting *fac*-tris(4-(2-pyridinyl)phenylpyridinato)iridium (**Ir1**) and 2-formylpyridine via a subcomponent self-assembly in the presence of $Zn(BF_4)_2{\cdot}6H_2O$ in acetonitrile under nitrogen (Figure **16a**).

Similarly, polyhedron **IrC3** was formed by mixing **Ir1** with 2-formylpyridine in the presence of $Co(ClO_4)\cdot 6H_2O$ in a 2:6:3 ratio in acetonitrile (Figure **17a**). Suitable single crystals for X-ray diffraction of both **IrC2** and **IrC3** were obtained by slow vapor diffusion of diethyl ether into MeCN solutions of the polyhedra. X-ray crystallography analyses revealed the formation of discrete cages of composition of Ir_2M_3 (where M is Zn in **IrC2** and Co in **IrC3**) that possessed a trigonal bipyramidal geometry. In both structures, the three M atoms form the equatorial plane and the two iridium atoms occupied the axial positions.

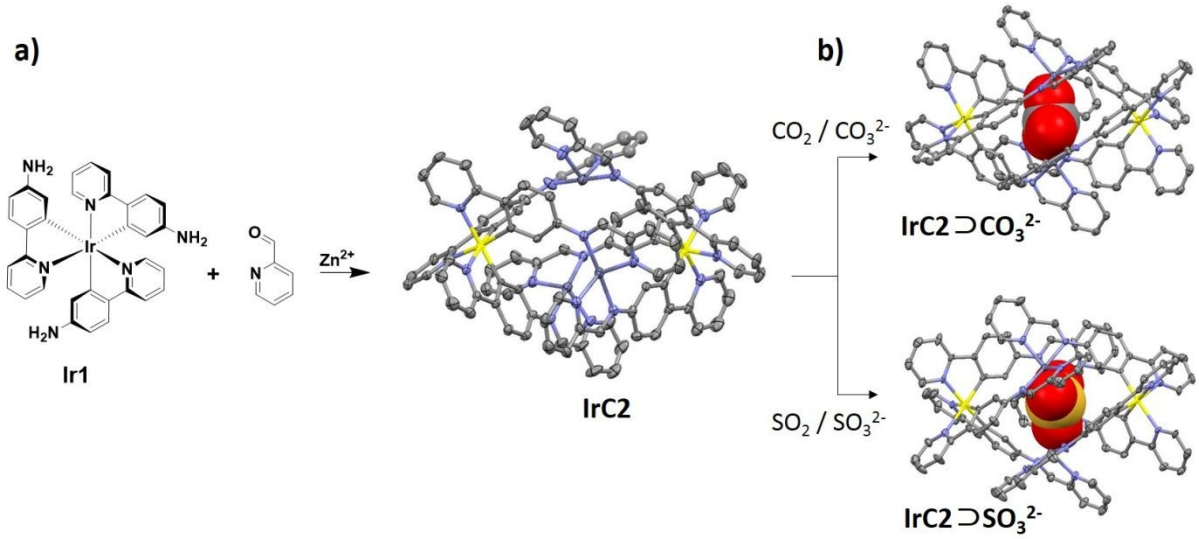

Figure **16**. **a)** formation of polyhedron **IrC2** from the assembly of **Ir1**. **b)** x-ray structures of **IrC2** encapsulating CO_3^{2-} and SO_3^{2-} shown with space-fill representations. Adapted with permission from Ref. [78].

Carbonic anhydrases (CAs) are enzymes that contain active Zn^{2+} sites that are coordinated to three histidine residues and a water or hydroxide molecule. In Nature, these enzymes catalyze the reversible hydration of CO_2 to CO_3^{2-}.[82] As **IrC2** exhibits an adequate hydrophobic cavity and coordination geometry around the Zn atoms to mimic the active site of natural CAs, its ability to convert CO_2 to CO_3^{2-} was investigated. Interestingly, vapor diffusion of diethyl

ether into a MeCN solution of **IrC2** under a CO_2 atmosphere yielded single crystals of **IrC2⊃CO_3^{2-}**. X-ray crystal structure analysis revealed that a molecule of CO_2 was successfully converted into CO_3^{2-} and encapsulated into the cavity of **IrC2** (Figure **16b**). **IrC2⊃CO_3^{2-}** exhibited the same polyhedral structure as **IrC2** with each of the three Zn atoms coordinating to one mono-dentate oxygen atom from CO_3^{2-} forming a [$Zn_3(\mu_3$-$CO_3^{2-})$] core, with CO_3^{2-} protected inside the cavity of the polyhedron. **IrC2** was found to be able to encapsulate also SO_2 and convert it into SO_3^-. The X-ray crystal structure of **IrC2** encapsulating **SO_3^{2-}** (**IrC2⊃SO_3^{2-}**, Figure **16b**) was obtained. Similar to **IrC2⊃CO_3^{2-}**, in **IrC2⊃SO_3^{2-}** the three Zn atoms coordinates to one mono-dentate oxygen atom from SO_3^{2-} forming a [$Zn_3(\mu_3$-$SO_3^{2-})$] core, which was encapsulated inside the cavity of **IrC2**. The formation of the host-guest systems **IrC2⊃CO_3^{2-}** and **IrC2⊃SO_3^{2-}** was observed not only in the crystal state but also in MeCN solution by ^{1}H NMR spectroscopy and ESI-mass spectrometry. Photoluminescence spectroscopy provided further evidence for the encapsulation of CO_3^{2-} within **IrC2**. As an example, upon pumping gaseous CO_2 into the MeCN solution of **IrC2**, the Ir(III)-centered emission at 508 nm was gradually quenched within 18 minutes, the result of the formation of **IrC2⊃CO_3^{2-}**.

The treatment of capsule **IrC3** with one equivalent of carbonate dianions in MeCN solution promoted the formation of the host-guest assembly **IrC3⊃CO_3^{2-}**, as observed both by X-ray diffraction (Figure **17**) and ESI-mass spectrometry. Interestingly, the empty cage **IrC3** was able to convert in high yield (86-96%) 2-aylpyridines to their α-trichloromethylated products when the system was photoirradiated using a 26 W fluorescent lamp (Figure **17b**). However, when **IrC3⊃CO_3^{2-}** or only the single components **Ir1** or $Co(ClO_4)_2{\cdot}6H_2O$ were tested as photocatalysts, no conversion was observed (Figure **17c**). These results unequivocally

demonstrate the photoconversion of 2-aylpyridines into their α-trichloromethylated products is only promoted when the Ir(III) chromophores are assembled with the coordinatively unsaturated Co(II) centers. In **IrC3**, the Ir(III) complexes are rigidly maintained in close proximity to the Co(II) metal ions, increasing the effective reaction concentration within the local micro-environment, and thus promoting high photoconversion of the substrates.

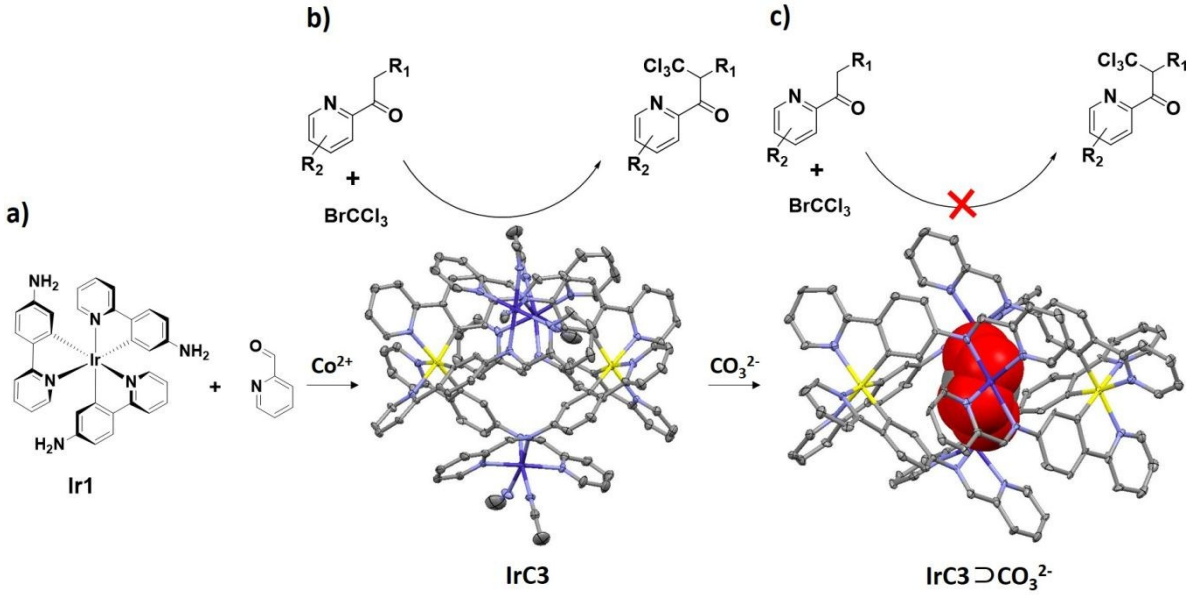

Figure **17**. **a)** Synthesis and X-ray crystal structure of polyhedral **IrC3**. **b)** illustration of the photocatalyzed α-trichloromethylation of acylpyridine promoted by **IrC3** (1 wt%). **c)** no photoreaction occurred when CO_3^{2-} ions was encapsulated into the cavity of **IrC3**. Adapted with permission from Ref. [78].

Ir(III) homochiral supramolecular cages of composition Λ_8-, Δ_8-, and *rac*-$[Ir_8Pd_4]^{16+}$ were recently reported by our group[83] through the self-assembly between two families of enantiopure[84] and racemic Ir(III) metalloligands of the form of Λ–, Δ–, and *rac*-$[Ir(C^N)_2(qpy)]BF_4$ and Pd^{2+} ions (Figure **18a**,**b**; C^N is mesppy = 2-phenyl-4-mesitylpyridinato in **Ir2**, and dFmesppy = 2-(4,6-difluorophenyl)-4-mesitylpyridinato in **Ir3**).

View Article Online
DOI: 10.1039/C8CC08327D

The assembly of ***rac*-Ir2** and ***rac*-Ir3** with Pd^{2+} afforded racemic cages of composition ***rac*-**$[Pd_4Ir_8]^{16+}$ (***rac*-IrC4** and ***rac*-IrC5**, respectively), while the assembly between Λ- and Δ-**Ir2** and Λ- and Δ-**Ir3** with Pd(II) ions gave rise to the enantiopure cages Λ_8- and Δ_8-$[Pd_4Ir_8]^{16+}$ (**Λ-, Δ-IrC4** and **Λ-, Δ-IrC5,** respectively). The chirality of the iridium metal did not impact the overall self-assembly process. Indeed, when either homochiral cage **Λ-** or **Δ-IrC4** was mixed with the homochiral cage **Δ-IrC5** at 85 ˚C for 12 h, metalloligand exchange was observed, promoting the formation of a statistical mixture of heteronuclear cages of composition $[Pd_4(\mathbf{\Lambda}, \mathbf{\Delta}\text{-}\mathbf{Ir2})_n(\mathbf{\Delta}\text{-}\mathbf{Ir3})_m](BF_4)_{16}$ (n + m = 8, from **Λ-**, **Δ-Ir2** : **Δ-Ir3** = 8 : 0 to **Λ-**, **Δ-Ir2** : **Δ-Ir3** = 0 : 8).

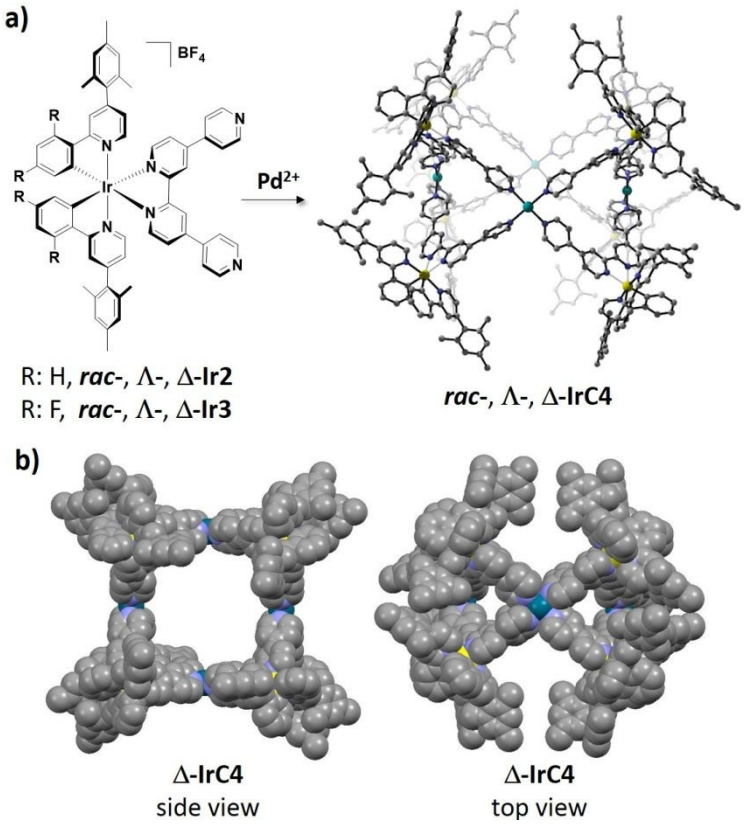

Figure **18**. **a)** Self-assembly between the metalloligands ***rac*-, Λ-, Δ-Ir2** and ***rac*-, Λ-, Δ-Ir3** and Pd^{2+} ions yielding cages ***rac*-, Λ-, Δ-IrC4** and ***rac*-, Λ-, Δ-IrC5.** For clarity, only the calculated structure of **Δ-IrC4** obtained is shown. **b)** View of the

structure of cage Δ-$[Pd_4\ Ir_8]^{16+}$, (side view on the left and top view on the right) with space-fill representation. Part **a)** is adapted with permission from Ref. [78].

The photophysical properties of the metalloligands ***rac***-, **Λ**-, **Δ-Ir2** and ***rac***-, **Λ**-, **Δ-Ir3**, and metallocages ***rac***-, **Λ**-, **Δ-IrC4** and ***rac***-, **Λ**-, **Δ-IrC5** were investigated both in DCM solution and in polymethyl methacrylate (PMMA) doped films (Figure **19**). The emissions of cages ***rac***-, **Λ**-, **Δ-IrC4** and ***rac***-, **Λ**-, **Δ-IrC5** in deaerated DCM were red-shifted, respectively, at 655 nm and 561 nm, with lower Φ_{PL} of 5% and 14%, and shorter τ_{PL} of 202 ns and 825 ns, compared to those of the corresponding metalloligands ***rac***-, **Λ**-, **Δ-Ir2** and ***rac***-, **Λ**-, **Δ-Ir3** (*e.g.,* ***rac*-Ir2**: λ_{PL} = 620 nm, Φ_{PL} = 14%, τ_{PL} = 300 ns; ***rac*-Ir3**: λ_{PL} = 527 nm, Φ_{PL} = 34%, τ_{PL} = 1000 ns). In the PMMA-thin films the emissions of **Ir2**, **Ir3**, **IrC4** and **IrC5** were blue-shifted, respectively, at 564 nm, 518 nm, 643 nm and 531 nm (Figures **19**), with enhanced Φ_{PL} of 28%, 41%, 10% and 16% and longer multi-exponential τ_{PL} compared to their photophysical behavior in DCM. This is the result of the less polar environment and the rigidification of **Ir2**, **Ir3**, **IrC4** and **IrC5** conferred by the PMMA polymer host. The emissions of the cages **IrC4** and **IrC5** in both DCM and PMMA-doped films are red-shifted compared to the corresponding metalloligands as a result of the coordination of the Lewis acidic Pd^{II} to the qpy ligand of **Ir2** and **Ir3**, thereby lowering their LUMO energies and giving rise to smaller optical gaps.[85]

View Article Online
DOI: 10.1039/C8CC08327D

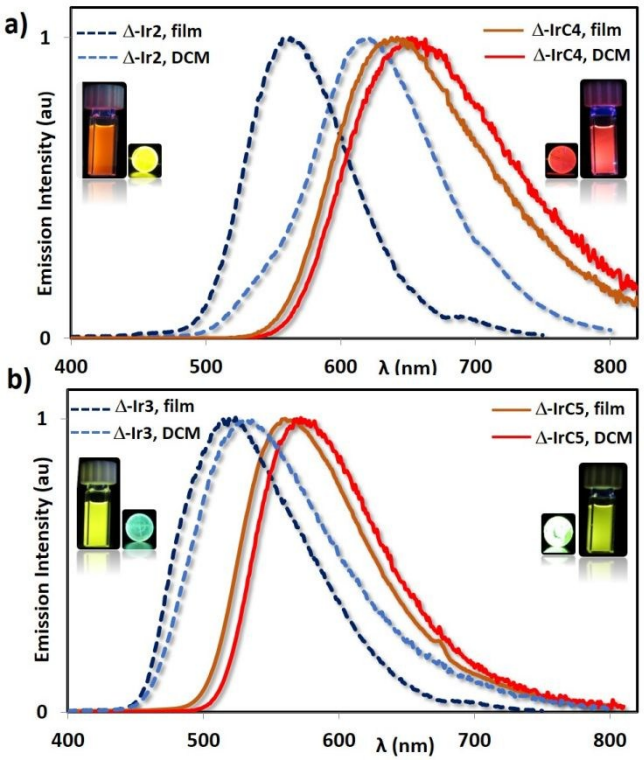

Figure **19**. Normalized emission spectra of: **a) Δ-Ir2** and **Δ-IrC4** and **b) Δ-Ir3** and **Δ-IrC5**. Dotted dark-blue lines: PMMA-doped film with 5 wt% of metalloligands **Δ-Ir2** and **Δ-Ir3** spin-coated on quartz substrates; Dotted light-blue lines: deaerated DCM solution of **Δ-Ir2** and **Δ-Ir3**; Solid orange lines: PMMA-doped film with 5 wt% of **Δ-IrC4** and **Δ-IrC5** spin-coated on quartz substrates; Solid red lines: deaerated DCM solution of **Δ-IrC4** and **Δ-IrC5**. Adapted with permission from Ref. [78].

The red-emitting cage **IrC4** (Figure **18b**) exhibited a diameter of approximately 18.8 Å (corresponding to the Pd···Pd distance) with an internal pocket volume of approximately 3480 Å^3, which was of adequate size to include mononuclear Ir(III) complexes. We therefore investigated the encapsulation of the anionic blue-emitting $NBu_4[Ir(dFppy)_2(CN)_2]$ complex (**Ir4**) and the subsequent photoinduced energy transfer between the blue-emitting guest donor **Ir4** and the red-emitting cage **IrC4** acceptor (Figure **20a**). The binding of **Ir4** within the cavity

of **IrC4** in **IrC4⊃Ir4** was confirmed by ^{1}H, ^{1}H DOSY and ^{19}F NMR investigations along with computational calculations, revealing an association constant *K* of $3.9 \times 10^{6} \pm 0.2$ M^{-1} for **IrC4⊃Ir4**.

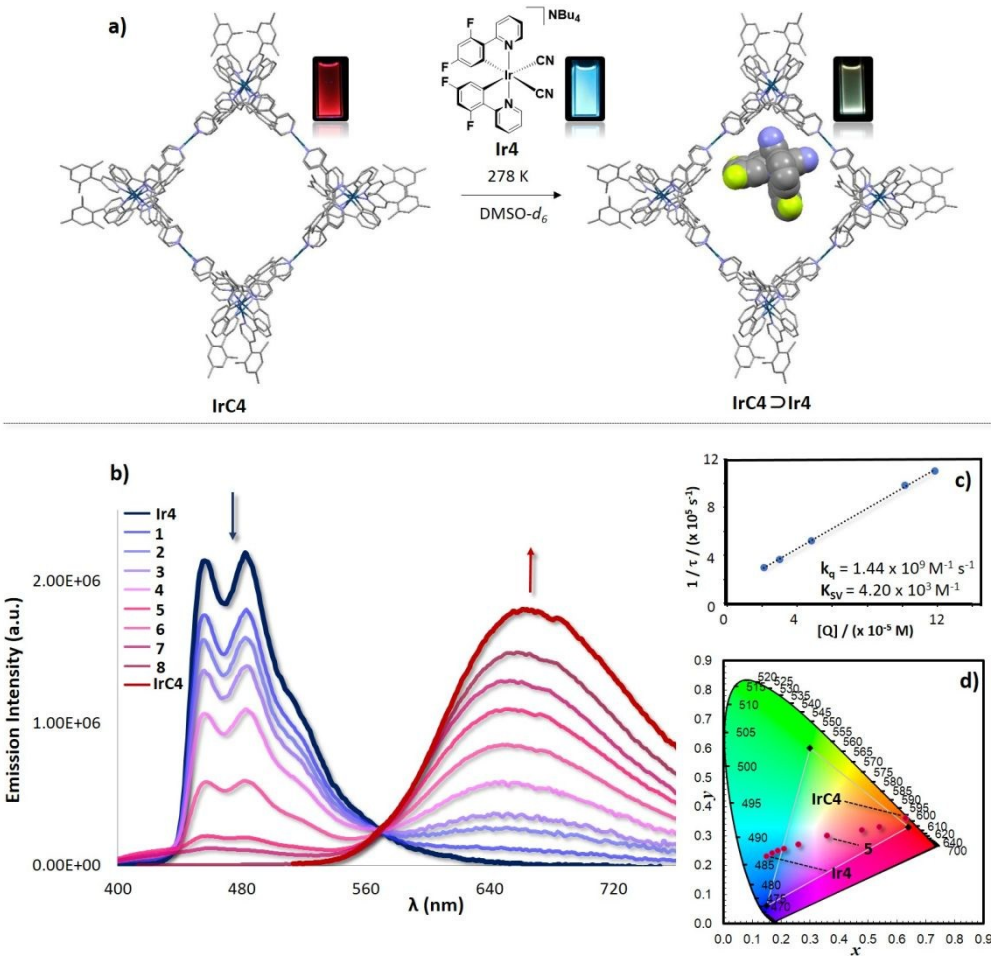

Figure **20**. **a)** Illustration of encapsulation of **Ir4** (space-fill representation) within the cavity of **IrC4**. The HF/6-31G(d) optimized host-guest structure **IrC4⊃Ir4** is illustrated. Insets are the emissions of the species under UV irradiation. **b)** Emission titrations of **IrC4** into a 100 μM solution of **Ir4** at 298 K in degassed DMSO; **c)** Stern-Volmer plot of the quenching study between **Ir4** and **IrC4**; **d)** CIE diagram indicating the change of emission colors during the emission titration. Adapted with permission from Ref. [78].

The ^{3}LC emission exhibited by complex **Ir4** in deaerated DMSO had two maxima at 458 and 483 nm and a shoulder at 515 nm (blue line in Figure **20b**), a Φ_{PL} of 52%, and a τ_{PL} of

View Article Online
DOI: 10.1039/C8CC08327D

2915 ns. When cage **IrC4** was titrated into a degassed DMSO solution of **Ir4** at 298 K, the blue emission of the donor **Ir4** was gradually quenched while the emission intensity of cage **IrC4** at 666 nm was gradually enhanced, showing an isosbestic point at 565 nm (Figure **20b**). Upon photoexcitation of **IrC4⊃Ir4** at 360 nm, efficient Dexter energy transfer from the blue-emitting **Ir4** to the red-emitting **IrC4** was therefore promoted with a calculated quenching rate constant (k_q) of 1.44×10^9 $M^{-1}s^{-1}$ and a Stern-Volmer constant (K_{SV}) of 4.20×10^3 M^{-1}. The CIE diagram in Figure **20d** shows the change in the emission colors observed during the emission titration. Titration 5 (Figure **20d**) shows CIE coordinates of (0.36, 0.30), which are close to the CIE coordinates of pure white light (0.31, 0.33).

Unlike the previous examples where the Ir-based metalloligands self-assemble in the presence of exogenous metal ions, Hardie, Zysman-Colman and co-workers[86] reported the self-assembly between two CTV-type ligands (CTV is cyclotriveratrylene), (±)-*tris*(isonicotinoyl)-cyclotriguaiacylene (**3**), and (±)-*tris*(4-pyridyl-methyl)-cyclotriguaiacylene (**4**), with *rac*-$[Ir(ppy)_2(NCMe)_2]^+$, forming metallo-cryptophane cages of compositions $[(Ir(ppy)_3)_3(\mathbf{3})_2](BF_4)_3$ (**IrC5**) and $[(Ir(ppy)_3)_3(\mathbf{4})_2](BF_4)_3$ (**IrC6**, Figure **21**). In these cages, it is the iridium centres themselves that act as vertices of the cages. Single crystals of **IrC5** suitable for x-ray diffraction were obtained (Figure **21b**) upon slow addition of diethyl ether to a nitromethane solution of **IrC5**. Cage **IrC5** exhibits three pseudo-octahedrally coordinated Ir(III) centers, each bearing two ppy ligands and two pyridyl groups from two ligands **3** disposed in a *cis*-arrangements. The two ligands **3** are bridged between three Ir(III) centers, acting as vertices. Interestingly, the cage exhibits homochiral self-sorting. Indeed, despite the reaction mixture containing both the iridium-centered Λ- and Δ-enantiomers and the M and P enantiomers of the CTV ligands, thereby potentially generating twelve possible stereoisomeric cages, only the enantiomeric MM-ΛΛΛ and PP-ΔΔΔ cages were observed

both in the x-ray structure of **IrC5** and by NMR in solution after several months, where the self-sorting was found to be very slow. The self-sorting of the racemic cages **IrC5** and **IrC6** in nitromethane solution was accelerated by the presence of chiral guests such as R-camphor or S-camphor but the self-sorting rate was not affected by the presence of an achiral adamantane guest. The self-assembly in $MeNO_2$ between the matched pair Δ-$[Ir(ppy)_2(NCMe)_2]^+$ and P-**3** or Λ-$[Ir(ppy)_2(NCMe)_2]^+$ and M-**3** yielded in less than five hours homochiral cages of composition Δ_3, M_2-$[(Ir(ppy)_3)_3(\mathbf{3})_2](BF_4)_3$ and Λ_3, P_2-$[(Ir(ppy)_3)_3(\mathbf{3})_2](BF_4)_3$, the formation of which was monitored by ^1H NMR spectroscopy.

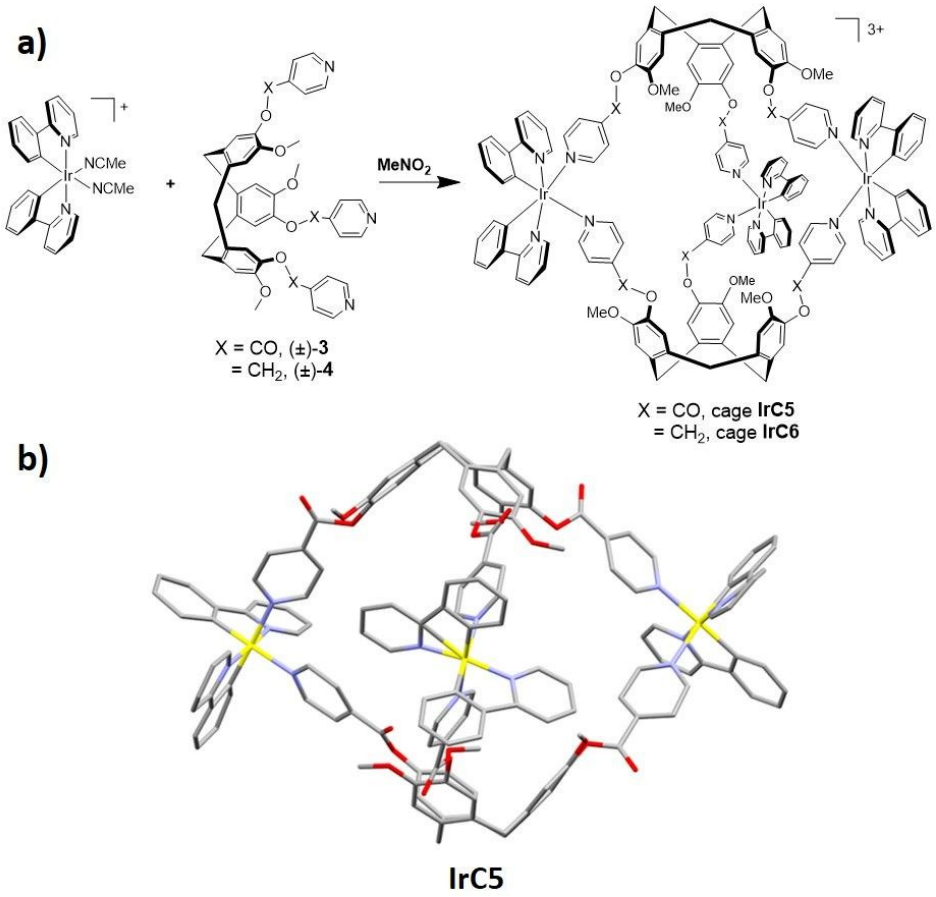

Figure **21**. **a)** Chemicals structures of ligands **3** and **4** and cages **IrC5** and **IrC6**. **b)** X-ray structure of cage **IrC5**. Part **a)** is adapted with permission from Ref. [78].

The emission properties of cages **IrC5** and **IrC6** in solution, as bulk powders and in PMMA-doped films (Figure **22a**, **b**) were investigated. **IrC6** exhibited a vibronic ^{3}LC emission at similar energies in DCM, as a powder and in PMMA-doped films (Figure **22b**) with Φ_{PL}, respectively, of 15%, 1.6% and 10% and biexponential τ_{PL}, respectively, of 523, 887ns; 141, 1175 ns and 688, 3042 ns. **IrC5**, on the other hand, exhibited a red-shifted emission (λ_{PL} = 648 nm) in the powder compared to that in DCM (λ_{PL} = 604 nm). In both media low Φ_{PL} of 1% and short bi-exponential emission decays were observed (τ_{PL} = 59, 129 ns in DCM and τ_{PL} = 55, 203 ns). The acyl linker in **IrC5** increased the conjugation of the iridium chromophore into the CTV scaffold resulting in a red-shifted emission compared to that observed for **IrC6**, but with similar photophysical properties compared to the monomeric reference complex $[Ir(ppy)_2(4\text{-}pyCO_2Et)_2]^+$ (4-pyCO$_2$Et = 4-ethyl isonicotinate) (λ_{PL} = 560 nm; Φ_{PL} = 2%).[87] As a result of the attenuation of non-radiative vibrational motion in PMMA-doped thin films, the emission of **IrC6** in thin film was blue-shifted and more structured at λ_{PL} = 514 nm with a higher Φ_{PL} and longer τ_{PL} (Φ_{PL} = 5.5%, τ_{PL} = 634 ns, 2319 ns) compared to those collected in DCM.

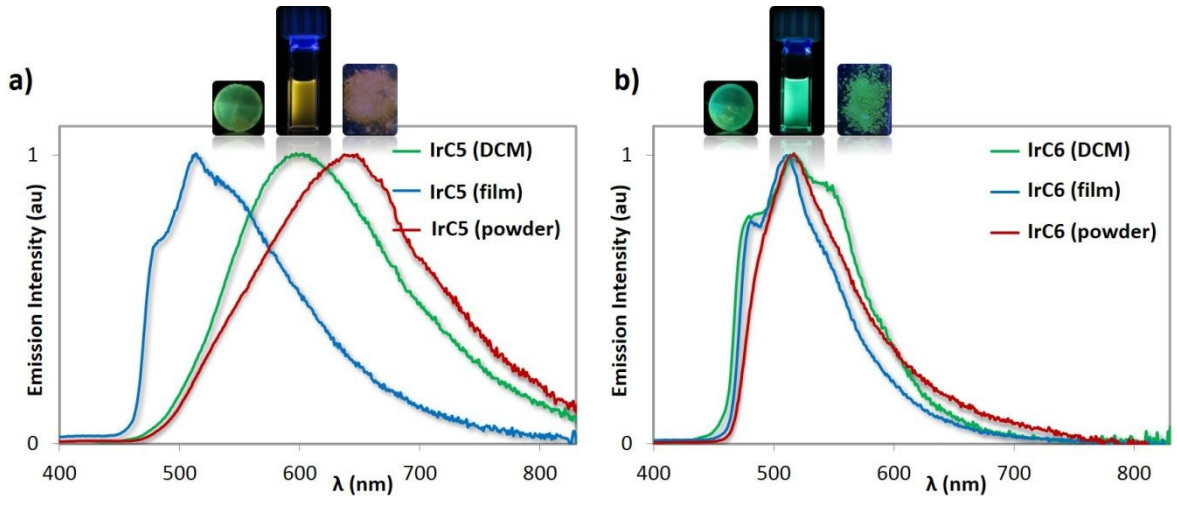

Figure **22**. Normalized photoluminescence spectra of **a) IrC5** and **b) IrC6**. Green lines are deaerated DCM solutions, light-blue lines are PMMA-doped films with 5wt% of cages spin-coated on a quartz substrate; red lines are bulk powders. Insets are images of the samples under UV irradiation. Adapted with permission from Ref. [78].

View Article Online
DOI: 10.1039/C8CC08327D

In a follow-up report the groups of Hardie and Zysman-Colman[88] reported a series of five iridium cages of the form of $[(Ir(C^N)_2)_3(L)_2]^{3+}$ where the C^N ligands are 2-phenylpyridinato, 2-(4-methylphenyl)-pyridinato or 2-(4,5,6-trifluorophenyl)pyridinato and L are two CTV ligands functionalized with 3- or 4-pyridyl-azo-phenyl units (Figure **23**). Interestingly, photoirradiation of these cages with a high-power laser result in E → Z photoisomerization of the pyridyl-azo-phenyl groups with up to 40% of groups isomerizing. The isomerization was found to be reversible upon exposure of the cages to blue light. Thus, the cages show reversible structure-switching while maintaining their compositional integrity (Figure **23b**).

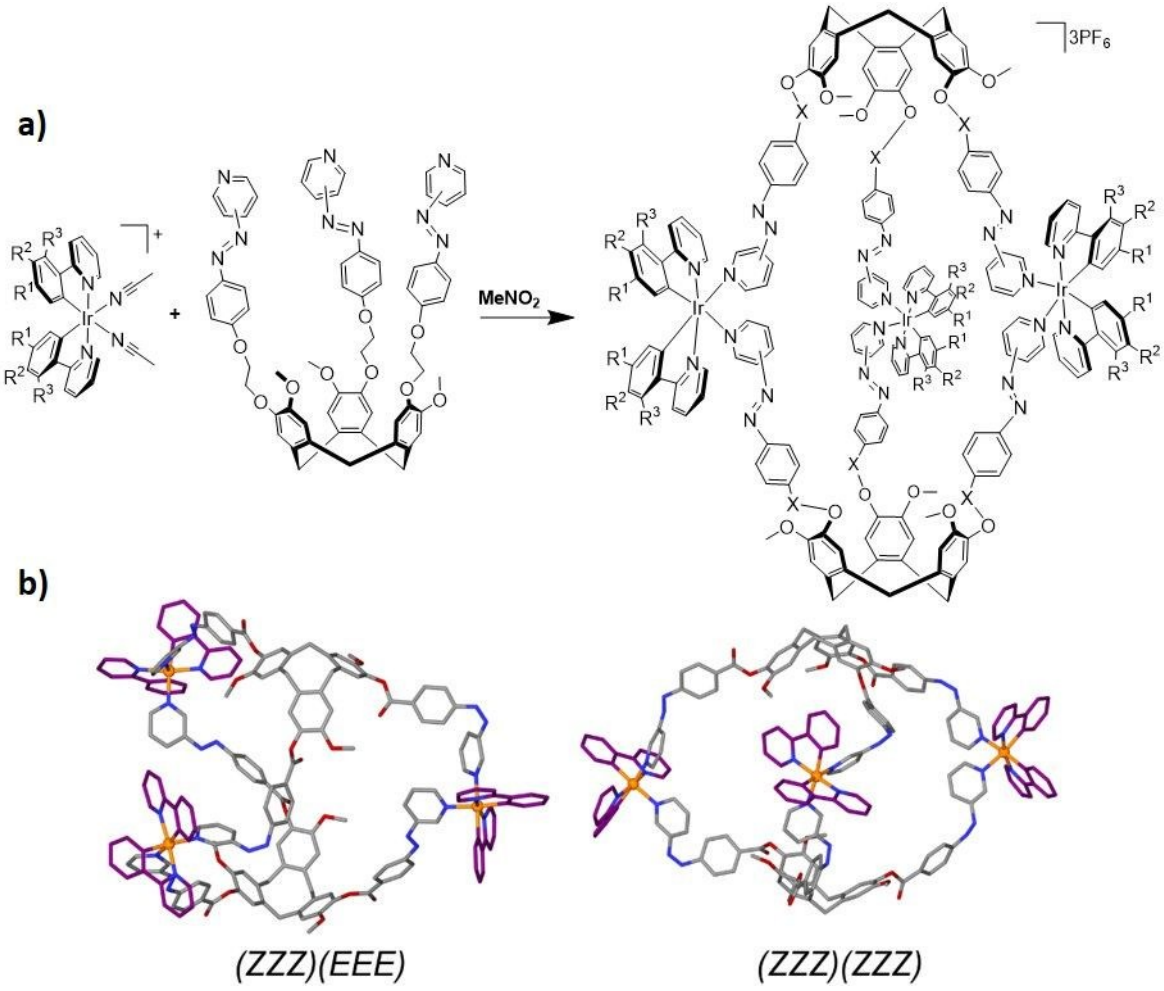

Figure **23**. **a)** Synthesis of $[(Ir(C^N)_2)_3(L)_2]^{3+}$ cages and **b)** energy-minimized models of $[(Ir(ppy)_2)_3(L)_2]^{3+}$ with three and six azo-units in *cis* (Z) conformation. Adapted with permission from Ref.[88] – Published by The Royal Society of Chemistry.

All cages exhibited similar deep blue structured emissions in DCM with maxima between 410 nm and 414 nm, albeit with low Φ_{PL} of around 1%. These emissions are significantly bluer compared to those of **IrC5** and **IrC6**, which showed, respectively, yellow/orange emission and cyan emission in DCM (Figure **22**). Similar to complexes of composition $[Ir(C^N)_2(bpy\text{-}AZB)]^+$, where bpy-AZB is a 2,2′-bipyridine (bpy) bearing azobenzene groups at the 4,4′-positions,[89] the HOMOs of the azo-cages are located on the $[Ir(C^N)_2]$ moieties while the LUMOs lie on the high-energy azobenzene fragment. Therefore, the presence of the azobenzene units attached to coordinating pyridines implicate large HOMO-LUMO gaps and account for the deep-blue emissions exhibited by these cages. These cages exhibited the bluest emissions reported to date for iridium-based metallosupramolecular cages. On the other hand, their low Φ_{PL} values are probably the result of concomitant population of emissive π* orbital involving the azobenzene ligand, access to non-radiative higher-lying metal-centered (MC) *d-d* states, which are located at similar energies, and non-radiative pathways associated with the conformationally flexible CTG-based ligands.[90]

In contrast to the weak red emissions exhibited by ruthenium assemblies, iridium(III) cages exhibit highly tunable emission colors which span from deep-blue to orange. The emission properties of these cage structures strongly depend on the nature of the iridium(III) complexes used in the self-assembly. We have herein illustrated that cages incorporating high-energy LUMO iridium complexes bearing azo-benzene fragments exhibit deep-blue emission, whereas cages incorporating lower-energy LUMO iridium complexes bearing a quaterpyridine

View Article Online
DOI: 10.1039/C8CC08327D

ligand scaffold are yellow or orange emissive. This high degree of color tunability coupled with the relatively high Φ_{PL} and short τ_{PL} exhibited by these iridium species make this class of compounds very interesting both as supramolecular photocatalysts and as emissive materials for lighting applications.

Conclusions

The self-assembly of arrays of Ru(II) and Ir(III) transition metal complexes in coordination metallocages clearly offers the great potential of combining the inherent guest-binding abilities of cage compounds with the redox- and photo-activity of phosphorescent metal complexes. In this feature article we have shown that such photoactive cages can be used as photocatalysts for hydrogen production and catalytic regio- and enantioselective photo-transformations of bound guests. Furthermore, the encapsulation of photoactive guests within phosphorescent cages permits a further modulation of the optoelectronic properties of the assemblies as a function of their photophysical interactions. This give rise to assemblies that exhibit emergent photophysical properties that are difficult to obtain in conventional molecular materials. Our contribution to the field has involved the investigation of four families of supramolecular cage compound containing Ru(II) (one family) and Ir(III) (three families) luminophores. We have investigated the photophysical properties of these systems both in solution and in the solid-state, and shown that the cages exhibit red-shifted emissions often with slightly lower Φ_{PL} and shorter τ_{PL} compared to the corresponding phosphorescent metalloligands. In the examples of heterometallic cages containing Ru(II) or Ir(III) metalloligands complexes to Pd(II) ions, partial quenching is due to the formation of lower-energy charge-transfer states that involve both the photoactive metalloligand and the Pd centers. On the other hand, when the phosphorescent metal complexes are electronically isolated from the ligand frameworks

involved in the self-assembly process, the photophysical properties of the luminescent complexes are generally maintained also in the assembled structure. Ligand design and control and preservation of the luminescent properties of the metal arrays in the assembled structures remain a major challenge to meet in order to expand the scope and use of photoactive cages. There is, however, little doubt that cage structures based on photoactive noble metals will continue to attract increasing attention and will play active roles in both functional supramolecular chemistry and in material science.

Acknowledgements. EZ-C acknowledges the University of St Andrews for financial support and the Engineering and Physical Sciences Research Council for financial support (EP/M02105X/1).

References

(1). (a) L. Chen, Q. Chen, M. Wu, F. Jiang and M. Hong, *Acc Chem Res*, 2015, **48**, 201-210; (b) H. Amouri, C. Desmarets and J. Moussa, *Chem Rev*, 2012, **112**, 2015-2041; (c) M. D. Ward and P. R. Raithby, *Chem. Soc. Rev.*, 2013, **42**, 1619-1636; (d) W. Wang, Y. X. Wang and H. B. Yang, *Chem Soc Rev*, 2016, **45**, 2656-2693.
(2). (a) R. Chakrabarty, P. S. Mukherjee and P. J. Stang, *Chem. Rev.*, 2011, **111**, 6810-6918; (b) T. R. Cook, Y.-R. Zheng and P. J. Stang, *Chem. Rev.*, 2013, **113**, 734-777.
(3). J.-M. Lehn, A. Rigault, J. Siegel, J. Harrowfield, B. Chevrier and D. Moras, *Proc. Natl. Acad. Sci. USA*, 1987, **84**, 2565.
(4). S. R. Seidel and P. J. Stang, *Acc. Chem. Res.*, 2002, **35**, 972-983.
(5). Q.-F. Sun, J. Iwasa, D. Ogawa, Y. Ishido, S. Sato, T. Ozeki, Y. Sei, K. Yamaguchi and M. Fujita, *Science*, 2010, **328**, 1144-1147.
(6). D. L. Caulder and K. N. Raymond, *Acc. Chem. Res.*, 1999, **32**, 975-982.
(7). I. Eryazici, C. N. Moorefield and G. R. Newkome, *Chem. Rev.*, 2008, **108**, 1834-1895.

(8). M. M. J. Smulders, I. A. Riddell, C. Browne and J. R. Nitschke, *Chem. Soc. Rev.*, 2013, **42**, 1728-1754.
(9). (a) N. C. Gianneschi, M. S. Masar and C. A. Mirkin, *Acc. Chem. Res.*, 2005, **38**, 825-837; (b) C.-C. You and F. Würthner, *J. Am. Chem. Soc.*, 2003, **125**, 9716-9725; (c) H. Hofmeier and U. S. Schubert, *Chem Soc Rev*, 2004, **33**, 373-399; (d) M. D. Ward, J. A. McCleverty and J. C. Jeffery, *Coord. Chem. Rev.*, 2001, **222**, 251-272; (e) J. J. Henkelis and M. J. Hardie, *Chem. Commun.*, 2015, **51**, 11929-11943; (f) D. A. McMorran and P. J. Steel, *Angew. Chem. Int. Ed.*, 1998, **37**, 3295-3297.
(10). M. Fujita, D. Oguro, M. Miyazawa, H. Oka, K. Yamaguchi and K. Ogura, *Nature*, 1995, **378**, 469-471.
(11). (a) D. Samanta and P. S. Mukherjee, *Chemistry*, 2014, **20**, 12483-12492; (b) D. Preston, S. M. McNeill, J. E. Lewis, G. I. Giles and J. D. Crowley, *Dalton Trans*, 2016, **45**, 8050-8060; (c) W. M. Bloch, Y. Abe, J. J. Holstein, C. M. Wandtke, B. Dittrich and G. H. Clever, *J. Am. Chem. Soc.*, 2016, **138**, 13750-13755; (d) D. K. Chand, K. Biradha, M. Fujita, S. Sakamoto and K. Yamaguchi, *Chem. Commun.*, 2002, 2486-2487; (e) S. Mukherjee and P. S. Mukherjee, *Chem. Commun.*, 2014, **50**, 2239-2248; (f) M. Han, D. M. Engelhard and G. H. Clever, *Chem Soc Rev*, 2014, **43**, 1848-1860.
(12). J. K. Klosterman, M. Iwamura, T. Tahara and M. Fujita, *J. Am. Chem. Soc.*, 2009, **131**, 9478-9479.
(13). D. Fujita, H. Yokoyama, Y. Ueda, S. Sato and M. Fujita, *Angew Chem Int Ed Engl*, 2015, **54**, 155-158.
(14). D. Fujita, Y. Ueda, S. Sato, H. Yokoyama, N. Mizuno, T. Kumasaka and M. Fujita, *Chem*, 2016, **1**, 91-101.
(15). N. Ahmad, H. A. Younus, A. H. Chughtai and F. Verpoort, *Chem Soc Rev*, 2015, **44**, 9-25.
(16). (a) M. Yoshizawa, J. K. Klosterman and M. Fujita, *Angew. Chem. Int. Ed.*, 2009, **48**, 3418-3438; (b) T. Furusawa, M. Kawano and M. Fujita, *Angew. Chem. Int. Ed.*, 2007, **46**, 5717-5719; (c) T. Yamaguchi and M. Fujita, *Angew Chem Int Ed Engl*, 2008, **47**, 2067-2069; (d) Y. Nishioka, T. Yamaguchi, M. Yoshizawa and M. Fujita, *J. Am. Chem. Soc.*, 2007, **129**, 7000-7001.
(17). (a) I. A. Riddell, M. M. Smulders, J. K. Clegg and J. R. Nitschke, *Chem. Commun.*, 2011, **47**, 457-459; (b) T. K. Ronson, S. Zarra, S. P. Black and J. R. Nitschke, *Chem. Commun.*, 2013, **49**, 2476-2490; (c) S. Zarra, D. M. Wood, D. A. Roberts and J. R. Nitschke, *Chem Soc Rev*, 2015, **44**, 419-432; (d) A. Galan and P. Ballester, *Chem Soc Rev*, 2016, **45**, 1720-1737; (e) H. Vardhan and F. Verpoort, *Adv. Synth. Catal.*, 2015, **357**, 1351-1368; (f) D. Fiedler, R. G. Bergman and K. N. Raymond, *Angew Chem Int Ed Engl*, 2006, **45**, 745-748.
(18). (a) A. Schmidt, V. Molano, M. Hollering, A. Pothig, A. Casini and F. E. Kuhn, *Chemistry*, 2016, **22**, 2253-2256; (b) A. Ahmedova, R. Mihaylova, D. Momekova, P. Shestakova, S. Stoykova, J. Zaharieva, M. Yamashina, G. Momekov, M. Akita and M. Yoshizawa, *Dalton Trans*, 2016, **45**, 13214-13221; (c) A. Mishra, S. Chang Lee, N. Kaushik, T. R. Cook, E. H. Choi, N. Kumar

Kaushik, P. J. Stang and K. W. Chi, *Chemistry*, 2014, **20**, 14401-14420; (d) B. Therrien, G. Süss-Fink, P. Govindaswamy, A. K. Renfrew and P. J. Dyson, *Angew. Chem. Int. Ed.*, 2008, **47**, 3773-3776; (e) J. E. M. Lewis, E. L. Gavey, S. A. Cameron and J. D. Crowley, *Chem. Sci.*, 2012, **3**, 778-784.
(19). (a) P. P. Neelakandan, A. Jimenez and J. R. Nitschke, *Chem. Sci.*, 2014, **5**, 908-915; (b) D. P. August, G. S. Nichol and P. J. Lusby, *Angew Chem Int Ed Engl*, 2016, **55**, 15022-15026.
(20). (a) A. Schmidt, A. Casini and F. E. Kühn, *Coord. Chem. Rev.*, 2014, **275**, 19-36; (b) A. Ahmedova, D. Momekova, M. Yamashina, P. Shestakova, G. Momekov, M. Akita and M. Yoshizawa, *Chem Asian J*, 2016, **11**, 474-477.
(21). (a) M. W. Cooke, D. Chartrand and G. S. Hanan, *Coord. Chem. Rev.*, 2008, **252**, 903-921; (b) L. J. Chen, H. B. Yang and M. Shionoya, *Chem Soc Rev*, 2017, **46**, 2555-2576; (c) T. H. Noh and O.-S. Jung, *Acc. Chem. Res.*, 2016, **49**, 1835-1843.
(22). H.-B. Yang, K. Ghosh, Y. Zhao, B. H. Northrop, M. M. Lyndon, D. C. Muddiman, H. S. White and P. J. Stang, *J. Am. Chem. Soc.*, 2008, **130**, 839-841.
(23). H.-B. Yang, K. Ghosh, B. H. Northrop, Y.-R. Zheng, M. M. Lyndon, D. C. Muddiman and P. J. Stang, *J. Am. Chem. Soc.*, 2007, **129**, 14187-14189.
(24). X. Yan, B. Jiang, T. R. Cook, Y. Zhang, J. Li, Y. Yu, F. Huang, H. B. Yang and P. J. Stang, *J Am Chem Soc*, 2013, **135**, 16813-16816.
(25). C. Gutz, R. Hovorka, C. Klein, Q. Q. Jiang, C. Bannwarth, M. Engeser, C. Schmuck, W. Assenmacher, W. Mader, F. Topic, K. Rissanen, S. Grimme and A. Lutzen, *Angew Chem Int Ed Engl*, 2014, **53**, 1693-1698.
(26). (a) K. Kurihara, K. Yazaki, M. Akita and M. Yoshizawa, *Angew Chem Int Ed Engl*, 2017, **56**, 11360-11364; (b) K. Yazaki, S. Noda, Y. Tanaka, Y. Sei, M. Akita and M. Yoshizawa, *Angew. Chem. Int. Ed.*, 2016, **55**, 15031-15034.
(27). M. Krick, J. Holstein, C. Wurtele and G. H. Clever, *Chem. Commun.*, 2016, **52**, 10411-10414.
(28). M. Käseborn, J. J. Holstein, G. H. Clever and A. Lützen, *Angew. Chem. Int. Ed.*, 2018, **57**, 12171-12175.
(29). (a) P. D. Frischmann, K. Mahata and F. Wurthner, *Chem Soc Rev*, 2013, **42**, 1847-1870; (b) L. Xu, Y. X. Wang and H. B. Yang, *Dalton Trans*, 2015, **44**, 867-890; (c) M. D. Ward, in *Comprehensive Supramolecular Chemistry II*, ed. J. L. Atwood, Elsevier, Oxford, 2017, pp. 357-371.
(30). (a) H. Ding, X. Wu, M. Zeller, Y. Xie and C. Wang, *J Org Chem*, 2015, **80**, 9360-9364; (b) M. Otte, P. F. Kuijpers, O. Troeppner, I. Ivanovic-Burmazovic, J. N. Reek and B. de Bruin, *Chemistry*, 2014, **20**, 4880-4884; (c) S. Durot, J. Taesch and V. Heitz, *Chem Rev*, 2014, **114**, 8542-8578.
(31). (a) P. D. Frischmann, V. Kunz and F. Wurthner, *Angew Chem Int Ed Engl*, 2015, **54**, 7285-7289; (b) Z. Li, N. Kishi, K. Hasegawa, M. Akita and M. Yoshizawa, *Chem. Commun.*, 2011, **47**, 8605-8607; (c) N. K. Al-Rasbi, C. Sabatini, F. Barigelletti and

M. D. Ward, *Dalton Trans*, 2006, 4769-4772; (d) A. Casini, B. Woods and M. Wenzel, *Inorg Chem*, 2017, **56**, 14715-14729.
(32). D. R. Martir, A. Pizzolante, D. Escudero, D. Jacquemin, S. L. Warriner and E. Zysman-Colman, *ACS Applied Energy Materials*, 2018, **1**, 2971-2978.
(33). M. L. Saha, X. Yan and P. J. Stang, *Acc Chem Res*, 2016, **49**, 2527-2539.
(34). (a) C. K. Prier, D. A. Rankic and D. W. C. MacMillan, *Chem. Rev.*, 2013, **113**, 5322-5363; (b) J. D. Blakemore, R. H. Crabtree and G. W. Brudvig, *Chem Rev*, 2015, **115**, 12974-13005.
(35). M. Grätzel, *J. Photochem. Photobiol., C*, 2003, **4**, 145-153.
(36). (a) H. Ozawa and K. Sakai, *Chem. Commun.*, 2011, **47**, 2227-2242; (b) A. R. Parent and K. Sakai, *ChemSusChem*, 2014, **7**, 2070-2080.
(37). L. Zeng, P. Gupta, Y. Chen, E. Wang, L. Ji, H. Chao and Z. S. Chen, *Chem Soc Rev*, 2017, **46**, 5771-5804.
(38). (a) C. Mari, V. Pierroz, S. Ferrari and G. Gasser, *Chem Sci*, 2015, **6**, 2660-2686; (b) M. Yang and U. Bierbach, *Eur. J. Inorg. Chem.*, 2017, **2017**, 1561-1572; (c) E. Alessio, *Eur. J. Inorg. Chem.*, 2017, **2017**, 1549-1560; (d) N. P. E. Barry and P. J. Sadler, *Chem. Commun.*, 2013, **49**, 5106-5131.
(39). (a) S. Campagna, F. Puntoriero, F. Nastasi, G. Bergamini and V. Balzani, in *Photochemistry and Photophysics of Coordination Compounds I*, eds. V. Balzani and S. Campagna, Springer Berlin Heidelberg, Berlin, Heidelberg, 2007, pp. 117-214; (b) I. M. Dixon, E. Lebon, P. Sutra and A. Igau, *Chem Soc Rev*, 2009, **38**, 1621-1634.
(40). (a) W. Sun, S. Li, B. Haupler, J. Liu, S. Jin, W. Steffen, U. S. Schubert, H. J. Butt, X. J. Liang and S. Wu, *Adv Mater*, 2017, **29**; (b) Y. Sun, Z. Chen, E. Puodziukynaite, D. M. Jenkins, J. R. Reynolds and K. S. Schanze, *Macromolecules*, 2012, **45**, 2632-2642; (c) C. Friebe, H. Görls, M. Jäger and U. S. Schubert, *Eur. J. Inorg. Chem.*, 2013, **2013**, 4191-4202.
(41). (a) W. Zhang, B. Li, H. Ma, L. Zhang, Y. Guan, Y. Zhang, X. Zhang, P. Jing and S. Yue, *ACS Appl Mater Interfaces*, 2016, **8**, 21465-21471; (b) R. Chen, J. Zhang, J. Chelora, Y. Xiong, S. V. Kershaw, K. F. Li, P. K. Lo, K. W. Cheah, A. L. Rogach, J. A. Zapien and C. S. Lee, *ACS Appl Mater Interfaces*, 2017, **9**, 5699-5708; (c) S. Zhang, L. Li, S. Zhao, Z. Sun and J. Luo, *Inorg Chem*, 2015, **54**, 8375-8379.
(42). (a) Y. F. Han, W. G. Jia, W. B. Yu and G. X. Jin, *Chem Soc Rev*, 2009, **38**, 3419-3434; (b) T. R. Cook, V. Vajpayee, M. H. Lee, P. J. Stang and K.-W. Chi, *Acc. Chem. Res.*, 2013, **46**, 2464-2474; (c) A. Schultz, X. Li, B. Barkakaty, C. N. Moorefield, C. Wesdemiotis and G. R. Newkome, *J Am Chem Soc*, 2012, **134**, 7672-7675.
(43). C. E. Hauke, A. N. Oldacre, C. R. P. Fulong, A. E. Friedman and T. R. Cook, *Inorg. Chem.*, 2017, **ASAP**, DOI: 10.1021/acs.inorgchem.1027b02657.

(44). C. E. Hauke, A. N. Oldacre, C. R. P. Fulong, A. E. Friedman and T. R. Cook, *Inorg. Chem.*, 2018, **57**, 3587-3595.
(45). T. Z. Xie, S. Y. Liao, K. Guo, X. Lu, X. Dong, M. Huang, C. N. Moorefield, S. Z. Cheng, X. Liu, C. Wesdemiotis and G. R. Newkome, *J Am Chem Soc*, 2014, **136**, 8165-8168.
(46). K. Li, L. Y. Zhang, C. Yan, S. C. Wei, M. Pan, L. Zhang and C. Y. Su, *J Am Chem Soc*, 2014, **136**, 4456-4459.
(47). K. Wu, K. Li, Y. J. Hou, M. Pan, L. Y. Zhang, L. Chen and C. Y. Su, *Nat Commun*, 2016, **7**, 10487.
(48). J. Guo, Y. W. Xu, K. Li, L. M. Xiao, S. Chen, K. Wu, X. D. Chen, Y. Z. Fan, J. M. Liu and C. Y. Su, *Angew Chem Int Ed Engl*, 2017, **56**, 3852-3856.
(49). M. Yoshizawa, Y. Takeyama, T. Okano and M. Fujita, *J. Am. Chem. Soc.*, 2003, **125**, 3243-3247.
(50). (a) S. Karthikeyan and V. Ramamurthy, *J. Org. Chem.*, 2006, **71**, 6409-6413; (b) Y. Nishioka, T. Yamaguchi, M. Kawano and M. Fujita, *J. Am. Chem. Soc.*, 2008, **130**, 8160-8161; (c) S. Karthikeyan and V. Ramamurthy, *J. Org. Chem.*, 2007, **72**, 452-458.
(51). M. Yoshizawa and M. Fujita, *Pure Appl. Chem.*, 2005, **77**.
(52). (a) M. Yoshizawa, S. Miyagi, M. Kawano, K. Ishiguro and M. Fujita, *J. Am. Chem. Soc.*, 2004, **126**, 9172-9173; (b) T. Murase, H. Takezawa and M. Fujita, *Chem. Commun.*, 2011, **47**, 10960-10962.
(53). (a) S. Rau, B. Schafer, D. Gleich, E. Anders, M. Rudolph, M. Friedrich, H. Gorls, W. Henry and J. G. Vos, *Angew Chem Int Ed Engl*, 2006, **45**, 6215-6218; (b) A. Fihri, V. Artero, M. Razavet, C. Baffert, W. Leibl and M. Fontecave, *Angew Chem Int Ed Engl*, 2008, **47**, 564-567.
(54). M. Hirahara, S. Masaoka and K. Sakai, *Dalton Trans.*, 2011, **40**, 3967-3978.
(55). A. N. Radhakrishnan, P. P. Rao, K. S. Linsa, M. Deepa and P. Koshy, *Dalton Trans*, 2011, **40**, 3839-3848.
(56). (a) T. A. White, S. L. Higgins, S. M. Arachchige and K. J. Brewer, *Angew Chem Int Ed Engl*, 2011, **50**, 12209-12213; (b) M. Elvington, J. Brown, S. M. Arachchige and K. J. Brewer, *J. Am. Chem. Soc.*, 2007, **129**, 10644-10645.
(57). H. Ozawa, M. Kobayashi, B. Balan, S. Masaoka and K. Sakai, *Chem Asian J*, 2010, **5**, 1860-1869.
(58). S. Chen, K. Li, F. Zhao, L. Zhang, M. Pan, Y. Z. Fan, J. Guo, J. Shi and C. Y. Su, *Nat Commun*, 2016, **7**, 13169.
(59). J. Yang, M. Bhadbhade, W. A. Donald, H. Iranmanesh, E. G. Moore, H. Yan and J. E. Beves, *Chem. Commun.*, 2015, **51**, 4465-4468.
(60). E. G. Moore, M. Benaglia, G. Bergamini and P. Ceroni, *Eur. J. Inorg. Chem.*, 2015, **2015**, 414-420.
(61). C. Shen, A. D. W. Kennedy, W. A. Donald, A. M. Torres, W. S. Price and J. E. Beves, *Inorg. Chim. Acta*, 2017, **458**, 122-128.
(62). D. Rota Martir, D. B. Cordes, A. M. Z. Slawin, D. Escudero, D. Jacquemin, S. L. Warriner and E. Zysman-Colman, *Chem. Commun.*, 2018, **54**, 6016-6019.

(63). E. T. Luis, H. Iranmanesh, K. S. A. Arachchige, W. A. Donald, G. Quach, E. G. Moore and J. E. Beves, *Inorg. Chem.*, 2018, **57**, 8476-8486.
(64). M. Chen, J. Wang, S. Chakraborty, D. Liu, Z. Jiang, Q. Liu, J. Yan, H. Zhong, G. R. Newkome and P. Wang, *Chem. Commun.*, 2017, **53**, 11087-11090.
(65). A. J. Metherell and M. D. Ward, *Chem. Commun.*, 2014, **50**, 6330-6332.
(66). (a) T. Kikuchi, S. Sato and M. Fujita, *J. Am. Chem. Soc.*, 2010, **132**, 15930-15932; (b) N. Kamiya, M. Tominaga, S. Sato and M. Fujita, *J. Am. Chem. Soc.*, 2007, **129**, 3816-3817; (c) J. E. Lewis, C. J. McAdam, M. G. Gardiner and J. D. Crowley, *Chem. Commun.*, 2013, **49**, 3398-3400.
(67). (a) T. Murase, S. Sato and M. Fujita, *Angew. Chem. Int. Ed.*, 2007, **46**, 1083-1085; (b) A. B. Elliott, J. E. Lewis, H. van der Salm, C. J. McAdam, J. D. Crowley and K. C. Gordon, *Inorg Chem*, 2016, **55**, 3440-3447; (c) J. E. M. Lewis, A. B. S. Elliott, C. J. McAdam, K. C. Gordon and J. D. Crowley, *Chem. Sci.*, 2014, **5**, 1833-1843; (d) A. M. Johnson, O. Moshe, A. S. Gamboa, B. W. Langloss, J. F. Limtiaco, C. K. Larive and R. J. Hooley, *Inorg Chem*, 2011, **50**, 9430-9442.
(68). (a) M. Wang, W. J. Lan, Y. R. Zheng, T. R. Cook, H. S. White and P. J. Stang, *J Am Chem Soc*, 2011, **133**, 10752-10755; (b) R. Chakrabarty and P. J. Stang, *J Am Chem Soc*, 2012, **134**, 14738-14741.
(69). W. K. Lo, G. S. Huff, J. R. Cubanski, A. D. Kennedy, C. J. McAdam, D. A. McMorran, K. C. Gordon and J. D. Crowley, *Inorg Chem*, 2015, **54**, 1572-1587.
(70). S. Hohloch, D. Schweinfurth, M. G. Sommer, F. Weisser, N. Deibel, F. Ehret and B. Sarkar, *Dalton Trans*, 2014, **43**, 4437-4450.
(71). A. Schmidt, M. Hollering, J. Han, A. Casini and F. E. Kuhn, *Dalton Trans*, 2016, **45**, 12297-12300.
(72). A. F. Henwood and E. Zysman-Colman, *Chem. Commun.*, 2017, **53**, 807-826.
(73). (a) D.-L. Ma, S. Lin, W. Wang, C. Yang and C.-H. Leung, *Chem. Sci.*, 2017, **8**, 878-889; (b) Y. You, S. Cho and W. Nam, *Inorg Chem*, 2014, **53**, 1804-1815.
(74). K. K.-W. Lo and K. K.-S. Tso, *Inorganic Chemistry Frontiers*, 2015, **2**, 510-524.
(75). (a) K. Teegardin, J. I. Day, J. Chan and J. Weaver, *Org. Process Res. Dev.*, 2016, **20**, 1156-1163; (b) T. Koike and M. Akita, *Inorganic Chemistry Frontiers*, 2014, **1**, 562-576.
(76). N. D. McDaniel and S. Bernhard, *Dalton Trans.*, 2010, **39**, 10021-10030.
(77). A. F. Henwood and E. Zysman-Colman, *Top. Curr. Chem.*, 2016, **374**, 36.
(78). D. Rota Martir and E. Zysman-Colman, *Coord. Chem. Rev.*, 2018, **364**, 86-117.

View Article Online
DOI: 10.1039/C8CC08327D

(79). O. Chepelin, J. Ujma, X. Wu, A. M. Z. Slawin, M. B. Pitak, S. J. Coles, J. Michel, A. C. Jones, P. E. Barran and P. J. Lusby, *J. Am. Chem. Soc.*, 2012, **134**, 19334-19337.
(80). X. Li, J. Wu, C. He, R. Zhang and C. Duan, *Chem. Commun.*, 2016, **52**, 5104-5107.
(81). X. Li, J. Wu, L. Chen, X. Zhong, C. He, R. Zhang and C. Duan, *Chem. Commun.*, 2016, **52**, 9628-9631.
(82). C. D. Boone, S. Gill, A. Habibzadegan and R. McKenna, *International Journal of Chemical Engineering*, 2013, **2013**, 1-6.
(83). D. Rota Martir, D. Escudero, D. Jacquemin, D. B. Cordes, A. M. Z. Slawin, H. A. Fruchtl, S. L. Warriner and E. Zysman-Colman, *Chem. Eur. J.*, 2017, **23**, 14358-14366.
(84). D. R. Martir, C. Momblona, A. Pertegás, D. B. Cordes, A. M. Z. Slawin, H. J. Bolink and E. Zysman-Colman, *ACS Applied Materials & Interfaces*, 2016, **8**, 33907-33915.
(85). D. Rota Martir, G. J. Hedley, D. B. Cordes, A. M. Z. Slawin, D. Escudero, D. Jacquemin, T. Kosikova, D. Philp, D. M. Dawson, S. E. Ashbrook, I. D. W. Samuel and E. Zysman-Colman, *Dalton Trans.*, 2016, **45**, 17195-17205.
(86). V. E. Pritchard, D. Rota Martir, S. Oldknow, S. Kai, S. Hiraoka, N. J. Cookson, E. Zysman-Colman and M. J. Hardie, *Chem. Eur. J.*, 2017, **23**, 6290-6294.
(87). W.-S. Sie, G.-H. Lee, K. Y.-D. Tsai, I. J. Chang and K.-B. Shiu, *J. Mol. Struct.*, 2008, **890**, 198-202.
(88). S. Oldknow, D. R. Martir, V. E. Pritchard, M. A. Blitz, Colin W. G. Fishwick, E. Zysman-Colman and M. J. Hardie, *Chem. Sci.*, 2018, DOI: 10.1039/C1038SC03499K.
(89). A. Telleria, J. Pérez-Miqueo, A. Altube, E. García-Lecina, A. de Cózar and Z. Freixa, *Organometallics*, 2015, **34**, 5513-5529.
(90). X. Gu, T. Fei, H. Zhang, H. Xu, B. Yang, Y. Ma and X. Liu, *J. Phys. Chem. A*, 2008, **112**, 8387-8393.

TOC graphic

View Article Online
DOI: 10.1039/C8CC08327D